20 Aug 2018

Modeling water flow in a Dutch polder network

Master's thesis to obtain the degree of Master of Science in Applied Mathematics at the Delft University of Technology

By R.J.J. Godefrooij




TU Delft

ACACIA WATER

Modeling water flow in a Dutch polder network

by

R.J.J. Godefrooij

to obtain the degree of Master of Science in Applied Mathematics at the Delft University of Technology,
to be defended publicly on 24 August 2018 at 2pm.

Student number:	4487427	
Project duration:	19 September 2017 – 24 August 2018	
Thesis committee:	Prof. dr. ir. C. Vuik,	TU Delft, supervisor
	Dr. ir. O. Hoes,	Acacia Water, supervisor
	Dr. H.M. Schuttelaars,	TU Delft

An electronic version of this thesis is available at `http://repository.tudelft.nl/`.

TU Delft Delft University of Technology

ACACIA WATER

Abstract

Agragrians in the Dutch Wadden sea region struggles with salinizing farmlands. Acacia Water's project Spaarwater enabled agrarians to measure salt concentrations in the ditches of their land using their mobile phone. All these measurements would ideally be used to evaluate the effects of salinization mitigation measures and to predict water quality over time. This gives rise to this thesis for an inquiry into a fast and simple surface water flow model which eventually could even be run on a mobile phone. The water model is a first necessary step for developing a water quality model with salt concentrations. The main focus of this thesis is on developing finite volume methods for the kinematic wave equation. It is a simplification of the full shallow water equations which are the governing equations for surface water flow. Finite volume methods for the diffusion wave equation and the full shallow water equations are also developed to serve as a comparison to the kinematic wave. It is shown that the kinematic wave and the diffusion wave have comparable features. Even though the kinematic wave is not the closest representation of reality, high computational gains could be made by using the kinematic wave equation instead of the full shallow water equations. For a simple straight ditch, the kinematic wave has shown to be 16 times faster than the full shallow water equations. For a network, however, it is not as straightforward. When comparing a kinematic wave network with a network in SOBEK, a software program that uses the full shallow water equations, the latter still has lower computational times.

Preface

Here it is, the final result of my year long immersion into the topic of surface water modeling. I stepped foot in Acacia Water's office on the 19th of September 2017 for the first time. A warm welcome was awaiting me in a team of about 25 hydrologists. Being unaware of the ins and outs of hydrological sciences, I spent the first months getting acquainted with these. I noticed it is a very complex scientific study since it combines many sciences such as physics, mathematics and chemistry. Not getting lost in all the possibly relevant information was an every continuing challenge during my thesis. It was a great learning experience for lowering my ever so high ambitions and for focusing on working step by step.

I would like to thank my TU Delft supervisor Professor Kees Vuik for his weekly supervision and his advice and ever so reassuring faith in me. I would like to thank my first Acacia Water supervisors Kyra Hu-a-ng and Jaco van der Gaast for getting me excited for studying hydrology and Olivier Hoes for smoothly taking over their supervisory role in the middle of the process. Thanks to to Henk Schuttelaars who took the time and honor to be the third thesis committee member. Last but not least, special thanks to my family, my Amsterfam and my close friends who are my best cheerleaders. Thank you for helping me through this year. Lots of love.

R.J.J. Godefrooij
Amsterdam, 20 August 2018

Contents

List of Figures

List of Symbols

a Acceleration in m/s^2

α_b Angle of the bottom slope with a given horizontal datum

B Channel width

C Chézy coefficient

c Wave celerity

D Hydraulic depth

g Gravitational constant

h Water depth; defined as the distance from the channel bottom to the water surface

I Water inflow from external sources

l_i Length of the i^{th} part of wetted area of the channel related to the wetted perimeter

L Channel length

m Mass

n_m Gauckler-Manning coefficient

P Wetted perimeter

q Discharge rate in m^3/s

R Hydraulic radius

ρ Fluid density

S_0 Channel bed clope

S_f Slope of the total energy line

S_p Pressure slope

τ_0 Bed shear stress

$\vec{u}(x,y,z)$ Flow velocity field

p Pressure

v Average cross sectional velocity

z_b The distance from given datum to bottom of the channel

1 Introduction

1.1. General

Agriculture in the Netherlands relies heavily on water management due to its polder landscape. A polder is a low-lying piece of land enclosed by dikes that is not naturally connected to outside water. Instead, its water surface levels are manually controlled. Particularly, the Wadden Sea coastal area has a shallow fresh water saline water surface level. Therefore, its agriculture relies on fresh rain water lenses floating on the saline groundwater. It is expected that these fresh water lenses will disappear in the future due to climate change, sea-level rise and land subsidence [1]. Hence the increasing water salinity results in salinization of the available water which can become damaging to the crops and their agricultural yield [2]. So how do we deal with salinization and how do we ensure the availability of clean fresh water?

A straightforward approach is to investigate the exact processes underlying fresh water losses and to subsequently find measures to reduce these losses. Important to note is that the effects of climate change on the salinization of Dutch agricultural areas is a relatively new research area. Knowledge on the effects of salinization on local levels is missing. Accordingly, more research is needed to predict future effects of climate change, sea-level rise and subsidence on the ground and surface water [3, 4]. For this reason, Acacia Water and the Waddenfonds started the project Spaarwater in 2013 to investigate mitigation measures for increasing salinization. The main mitigation measures researched in the Spaarwater project are as follows [1];

1. Establishing locally self-sufficient water supplies by either artifically managing groundwater recharge or by creating underground fresh water buffers
2. Enlarging the freshwater lenses through reducing salinization by system specific drainage
3. Implementing new irrigation methods, such as drip-irrigation, to use the available freshwater as efficiently as possible

The main aim is to safeguard and improve fresh water supplies, whilst taking the mitigation measures' technical and economic feasibility into account. The project is carried out in cooperation with multiple organizations such as provincial water authorities, provincial governments, agrarians and agricultural business organizations in the Dutch coastal Wadden Sea region. Altogether, there are four pilot locations in the Provinces of Noord-Holland, Friesland and Groningen [1].

1.2. Problem statement

The above-mentioned salinizing farmlands in the Dutch polders are the focus of this research. Acacia Water tests the effects of mitigation measures by determining the salinity of water with an electrical conductivity (EC) meter. Electrical conductivity easily translates to salt content. Therefore, an EC meter is a simple and quick tool for determining salinity levels. A great advantage is that farmers can also do these measurements themselves with a simple device connected to their mobile phone. Accordingly, they collect data about the water's salinity over time.

Acacia Water would like to use this data to develop a better understanding of the effects of implementing a mitigation measure. However, the water ditches in the farmlands are part of a complex network of water courses and it is labor intensive to check the progress of the effects of each of the mitigation measures on the land's salinization in space and time. Hence, there's the ambition to develop a web application with underlying mathematical tools to predict the local effects on salinity levels when introducing a mitigation measure. For doing so, the first idea is to simply connect the collected datapoints by interpolating the data. For interpolating the data, one needs to know about the water flow in the infrastructure of a ditches network. More specifically, one needs to know about the governing mathematical laws of the water flow.

1.3. Research objective

The goal of this study is to develop a water flow model for a ditches network in a Dutch polder. A variety of surface water models are available; think for example of SOBEK, HEC-RAS and FLOW-3D. In these programs, methods with high computational times are applied to model water flow in a very detailed manner. In contrast, this research aims to develop a model which gives a general idea of the global water flow in a network, rather than a very detailed account of local water flow in specific points of a ditch. Importantly, the model should be simple and have small computational times so that it eventually could run on a mobile phone. This research presents the starting point for a water flow model for a ditches network in a Dutch polder. Various methods are compared to enable a well-grounded decision on which approach to choose for further model development. The water flow model, in turn, serves as a starting point for a flow model which includes water quality and sediment transport.

1.4. Methods and structure

Important for the first design of the model is that it is simple and has small computational times whilst keeping in mind that complexities can be added later. Therefore, three possible approaches will be explored in to give an overview of the modeling options and to test for their applicability in a simple and fast water flow model. The methods have been implemented using Python 3.

The structure of this thesis report is as follows. Chapter 1 is this introductory chapter. Chapter 2 discusses the full shallow water equations which are the equations governing surface water flows in open channels. Chapter 3 gives the options for simplifying the shallow water equations. The three surface water modeling approaches discussed in this thesis are the kinematic wave, the diffusion wave and the dynamic wave. The numerical finite volume method for solving the kinematic wave equation on a straight channel is developed in Chapter 4. Then, in Chapter 5 the method developed in Chapter 4 is applied to the diffusion wave. Subsequently, Chapter 6 develops the numerical finite volume method for solving the dynamic wave, which is the same as the full shallow water equations. Chapter 7 gives an overview and comparison of the three different approaches. Then, in Chapter 8 the kinematic wave is applied to a small hypothetical ditches network which is accordingly compared to the same network implemented in SOBEK. Chapter 9 gives the conclusions and further recommendations.

2

The shallow water equations

2.1. General

A variety of different hydrological transport models were developed since the increase in the computer's computational power and the rising demands for detailed numerical forecasting. Hydrological transport models simulate stream flow and calculate water quality parameters, with varying modeling purposes; for example, groundwater transport, surface water flow, sediment transport and so forth. The focus lies on surface water modeling in this thesis, and more specifically, on open channel flow. Open channel flow entails the study of water flow with a free surface, which is subject to atmospheric pressure and is driven by gravity [5, 6]. Ultimately, we want to learn about the amount of water flowing past specific points in a ditch over time. Overall, we aim to learn about the water flow in the entirety of a ditches network; thus, we are focusing on the behavior of waves on large scales rather than local waves with turbulent flow. The design of a water flow model is the first and a necessary step for eventually getting an idea of the saline and fresh water flows in the entirety of a ditches network.

2.2. Derivation and interpretation

The shallow water equations are partial differential equations describing open channel flow, formulated as follows:

$$\begin{cases} \frac{\partial A}{\partial t} + \frac{\partial q}{\partial x} = I \\ \frac{\partial q}{\partial t} + \frac{\partial qv}{\partial x} = gA(S_0 - S_f - S_p) \end{cases} \tag{2.1}$$

Each of the terms in the equations will be explained in the following paragraphs. These equations have been derived from the more general Navier-Stokes equations describing the motion of viscous fluid substances. Analytical solutions to the the shallow water equations can only be found in extremely simplified forms. Hence, this led to the development of numerical techniques, such as the finite difference method or finite volume methods, to approximate solutions for the governing equations [5]. The shallow water equations consist of two partial differential equations describing the continuity and momentum principles.

2.2.1. Assumptions

The description of three dimensional open water waves in channels is given by :

The flow velocity field $\vec{u}(t,x,y,z)$
The pressures $p(t,x,y,z)$
The water depths $h(t,x,y)$

which results in a complex system with three variables varying in three or four dimensions. Hence, these dependencies need to be partly relaxed and simplified to enable open water flow calculations [7]. In this section basic definitions and assumptions are discussed which are commonly made to simplify the open water flow equations to describe the waves as one-dimensional in space. Thus, the variables mentioned above now become

The flow velocity $\vec{u}(t,x)$
The pressures $p(t,x,z)$
The water depths $h(t,x)$

Cross section For every position x along a channel, the *cross section* A is the unique plane perpendicular to the flow direction along the channel. A horizontal water level is assumed in each cross section and the geometry of each cross section is assumed to be known completely. Moreover, $z_b(x)$ denotes the lowest point of the cross section at x. The lowest point z_b is measured from an arbitrary horizontal zero fixed for the whole channel and usually taken to be sea level.

Wetted perimeter The *wetted perimeter* P is defined as the cross sectional area of the channel that touches the water, as is also illustrated in Figure 2.1. Mathematically, the wetted perimeter can be defined by

$$P = \sum_{i=0}^{\infty} l_i \tag{2.2}$$

where l_i is the length of each surface in contact with the water. Followingly, the *hydraulic radius* R and the *hydraulic depth* D are defined by

$$R = \frac{A}{P}$$
$$D = \frac{A}{B}$$

with A being the cross sectional area and B the channel width.

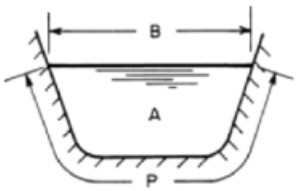

Figure 2.1: Sketch of the crossectional area of a channel as illustrated in [6]. P is the wetted perimeter, A the cross sectional area and B the channel width.

Discharge and average velocity The amount of water flowing through a particular cross section, at a given time, is determined by the velocity field $\vec{u}(t,x,y,z)$. Since we are focusing on large wavelengths and large scales, we are merely interested in the average velocity and total water flow in a cross section. To quantify

this, the *discharge* q is defined as the volumetric flow rate of water through a given cross sectional area A. It has a dimension of m^3/s. Mathematically, the discharge is given by

$$q(t,x) = \int\int_{(y,z)\in A} u_x(t,x,y,z)$$

which simplifies to

$$q(t,x) = A(t,x)v(t,x) \tag{2.3}$$

where $v(t,x)$ is the *average velocity*, over a given cross section $A(t,x)$, given by

$$v(t,x) = \frac{1}{A(t,x)} \int\int_{(y,z)\in A} u_x(t,x,y,z)$$

[7, 8].

Hydrostatic pressure Another important simplifying assumption is that of *hydrostatic pressure*, i.e. the pressure behaves the same as in still water. Again, this assumption is made because of the long waves. Hydrostatic pressure means that at every point in the river, the pressure equals the static pressure of the water column above. Hence, the pressure increases linearly from the top to the bottom of the channel [7]. The relationship between pressure p and height z is given by

$$p(t,x,z) = \rho g(h(t,x) - z) \tag{2.4}$$

where ρ is the volumetric mass density, g is the gravitational constant, $h(t,x)$ is the depth and z is the height of the point of consideration measured from the lowest bottom point z_b. Hence, the pressures for all the points in each cross section along the channel are known. Thus the pressure p is considered to be a given quantity.

External inflow The inflow from external processes outside of the system of the channel is incorporated in the source term $I(t,x)$. Processes such as rainfall, seepage or lateral inflow can be accounted for in this source term.

2.2.2. The continuity equation

The first partial differential equation in the shallow water equations is the continuity equation

$$\frac{\partial A}{\partial t} + \frac{\partial q}{\partial x} = I \tag{2.5}$$

The continuity equation is based on the conservation of mass principle; the amount of water flowing into a channel length equals the amount of water flowing out of that channel length. To illustrate this, let us consider an open channel without lateral inflow; meaning that there is no water flowing in from the sides of the river or from a reservoir. In this channel, consider a control volume with two cross sections 1 and 2, as illustrated in Figure 2.2.

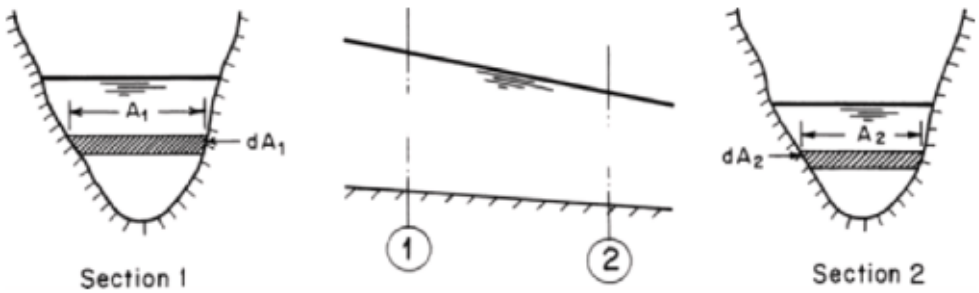

Figure 2.2: Sketch of flow between channel cross sections as illustrated in [6]

For this volume it must hold that in a specific time interval, Δt, the inflow volume equals the outflow volume. Usually, this principle is expressed in discharge q which is the volumetric flow rate of water that is transported through a given cross sectional area [9]. Simply said, the cross sectional area in section 1 is larger than in section 2. Therefore, the volumetric flow rate q is smaller at point 1 than at point 2.

Incorporating lateral inflow gives that the change in storage equals the sum of the lateral flow with the difference between inflow and outflow. These terms will be discussed in the preceding paragraphs.

Change in storage The *change in storage* is the change in mass in the control volume from time t to time $t+\Delta t$. With $\rho A(t,x)\Delta x$ being the mass in the control volume at time t, we get

$$\begin{aligned}\text{change in storage} &= \Delta x(\rho A(t+dt,x) - \rho A(t,x)) \\ &\approx \frac{\partial \rho A}{\partial t}(t,x)\Delta x \Delta t\end{aligned}$$

Difference between inflow and outflow The *difference between inflow and outflow* relates to the discharge $q(t,x)$. At x, the discharge flowing into the control volume is $q(t,x)$. Hence, the total amount of water entering the control volume between times t and $t+\Delta t$ equals $\Delta t \rho q(t,x)$. Over the control volume we get

$$\begin{aligned}\text{flow in - flow out} &= \Delta t(\rho q(t,x) - \rho q(t,x+\Delta x)) \\ &\approx -\frac{\partial \rho q(t,x)}{\partial x}\Delta x \Delta t\end{aligned}$$

Lateral flow $I(t,x)$ refers to the inflow or outflow of water outside of the river due events such as rainfall, seepage or evaporation. The total lateral flow into the control volume is specified by

$$\rho I(t,x)\Delta x \Delta t$$

where $I(t,x)$ can be taken as a constant or as a function of time and/or space.

Combining above terms gives the continuity equation given by

$$\text{change in storage} = \text{inflow - outflow} + \text{external flow}$$

$$\frac{\partial \rho A}{\partial t}(t,x)\Delta x \Delta t = -\frac{\partial \rho q(t,x)}{\partial x}\Delta x \Delta t + \rho I(t,x)\Delta x \Delta t$$

which can be simplified, by taking $\rho = 1$ constant for the density of water, to

$$\frac{\partial A}{\partial t}(t,x) = -\frac{\partial q(t,x)}{\partial x} + I(t,x)$$

hence resulting in the continuity equation (2.5).

2.2.3. Equation of motion

The second partial differential equation in the shallow water equations is the equation of motion

$$\frac{\partial q}{\partial t} + \frac{\partial q v}{\partial x} = gA(S_0 - S_f - S_p) \tag{2.6}$$

The equation of motion is based on the conservation of momentum principle. It describes the type of displacement of the water. In a similar manner to the continuity equation, the first term on the left hand side in equation (2.6) is the *local acceleration*, which is the change in momentum due to the change in velocity over time, corresponds to the storage in momentum and the second term is the *convective acceleration term*, which describes the change in momentum due to the change in velocity along the channel, corresponds to the difference between momentum inflow and momentum outflow. The terms on the right hand side of the equations relate to the external forces on the water; S_0 relates to the gravitational force, S_f relates to the friction force and S_p relates to the pressure force. The interpretation of each term in the equation of motion will be further explained in the following paragraphs.

Note that only the conservation of momentum in the x direction is considered, which is the direction of flow. Momentum is defined by mass times velocity; mv. Hence, the change in momentum is defined by

$$\frac{\partial mv}{\partial t} = m\frac{\partial v}{\partial t} = ma = F$$

where a is the acceleration and F the sum of the external forces in the x direction.

Change in storage of momentum In a similar manner as was discussed in the previous section, the mass in the control volume is defined as $\rho A(t,x)\Delta x$. Hence, the momentum is given by $\rho A(t,x)v(t,x) = \rho q(t,x)$ which gives a change in storage of momentum given by

$$\text{change in storage of momentum} = \rho\frac{\partial q(t,x)}{\partial t}$$

Difference between momentum inflow and momentum outflow In addition, the total amount of momentum in the control volume between t and $t+\Delta t$ equals $\Delta t q(t,x)v(t,x)$. Thus, we get

$$\begin{aligned}\text{momentum inflow} - \text{momentum outflow} &= \\ &= \Delta t[\rho q(t,x)v(t,x) - \rho q(t,x+\Delta x)v(t,x+\Delta x)] \\ &\approx -\rho\frac{\partial Q(t,x)v(t,x)}{\partial x}\Delta x\Delta t\end{aligned}$$

Accordingly, using $\rho = 1$, the equation of motion is written as

$$\frac{\partial q}{\partial t} + \frac{\partial q v}{\partial x} = F \tag{2.7}$$

where $F = F_{gravity} + F_{pressure} + F_{friction}$ is the sum of the external forces.

Gravitational force The total gravitational force F_g points down to the center of the earth and for the control volume it is given by

$$\begin{aligned} F_g &= -gm\hat{\mathbf{z}} \\ &= -g\rho A\Delta x\hat{\mathbf{z}} \end{aligned}$$

where $\hat{\mathbf{z}}$ denotes that the force is along the z axis which is the axis pointing up. Only the forces in the direction of flow are needed for the equation of motion. Hence, F_g is decomposed into two force components; namely, one in the direction of flow and one pointing down while being perpendicular to the direction of flow. The decomposition of the gravitational force is shown in Figure 2.3.

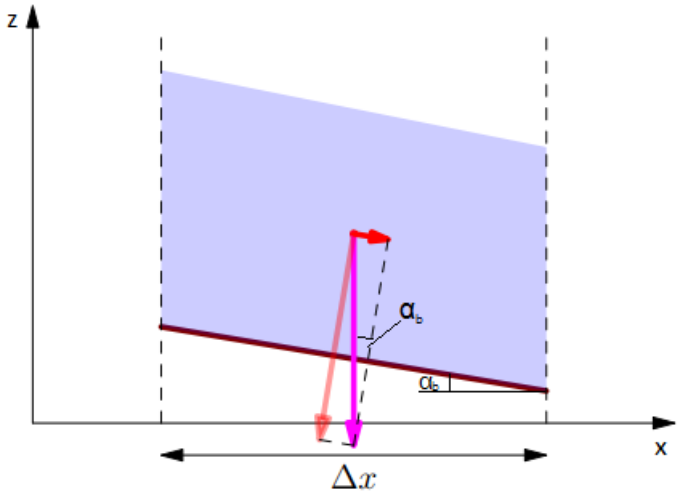

Figure 2.3: Decomposition of the gravitational force as illustrated in Figure 3.5 in [7]

Accordingly, by geometrical arguments using the angle α_b and the channel bed slope S_0 the force in the flow direction is derived, called F_0 for convenience

$$F_0 = \frac{\sin(\alpha_b)F_g}{\Delta x} = g\rho AS_0$$

where for small α_b it holds that $S_0 = \tan(\alpha_b) \approx \sin(\alpha_b) \approx \alpha_b$ [7].

Pressure force Pressure force can generate flow momentum even if the channel bed slope is zero. Hydrostatic pressure is assumed, hence pressure increases linearly with depth. Thus, all pressure forces are generated by the differences in depths between the left and right of the control volume.

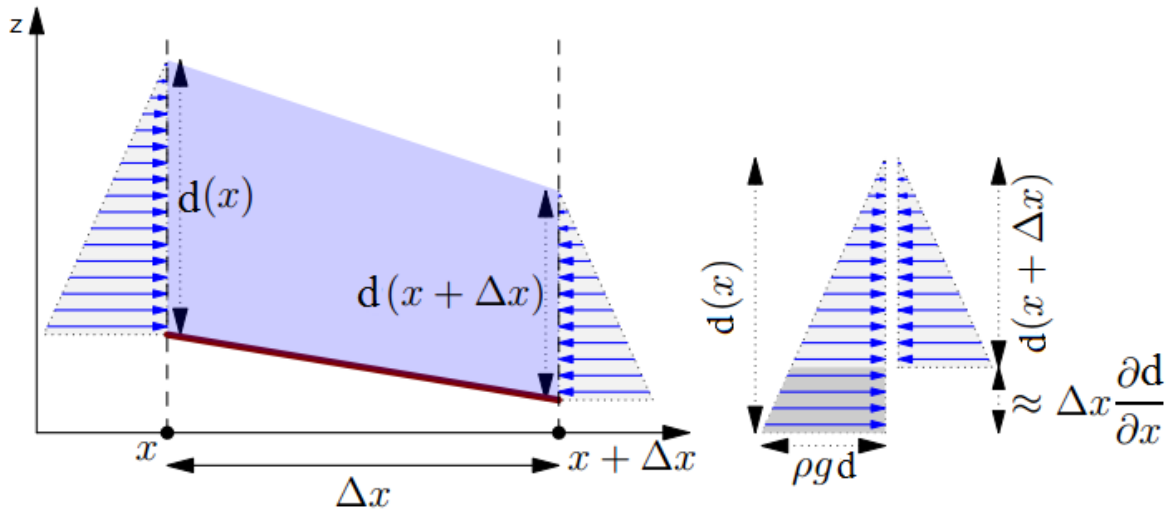

Figure 2.4: Graphical representation of the pressure forces on a control volume as illustrated in Figure 3.7 in [7]

As is shown in Figure 2.4, triangular pressure force fields exist due to hydrostatic pressure. Accordingly, the pressure force per unit length is calculated by evaluating the pressure differences between the cross sectional areas at x and $x+\Delta x$. Here, the y axis corresponds to the channel width.

$$\begin{aligned} F_p &= \frac{\rho g}{\Delta x}\int \mathrm{d}y \frac{h^2(x+\Delta x,y)-h^2(x,y)}{2} \\ &\approx \frac{\rho g}{-2\Delta x}\int \mathrm{d}y \frac{\partial h^2(x,y)}{\partial x} \\ &= -\frac{\rho g}{2\Delta x}\int \mathrm{d}y \Delta x[-2h(x,y)\frac{\partial h(x,y)}{\partial x}] \\ &= -\rho g \int \mathrm{d}y \frac{\partial h(x)}{\partial x} \\ &= -\rho g \frac{\partial h(x)}{\partial x} A = -\rho g A S_p \end{aligned}$$

where $\frac{\partial h(x)}{\partial x}$, the depth slope, is defined as the pressure slope S_p [7].

Friction force Flow loses momentum due to friction with the channel bed, plants, geographical structures, and so forth. Here, it is impossible to calculate the friction losses exactly because of the many different factors involved. Hence, the expressions for the friction force are highly empirical. Frictional forces created by the shear stress along the bottom and the sides of the control volume are given by $-\tau_0 P \mathrm{d}x$ as derived by Chow [8], where τ_0 is the bed shear stress and P is the wetted perimeter. With $\tau_0 = \rho g \frac{A}{P} S_f$. Hence, similarly to the gravitational and the pressure forces, the friction force also takes the form

$$F_f = -\rho g A S_f$$

As will be discussed in Section 3.2.1, S_f is the total energy gradient and can be determined empirically using Manning's Equation. Hence, plugging in each of these force terms into (2.7) results in the full equation of motion (2.6). Equation (2.6) can be simplified to the other, simpler types of flow by leaving out specific terms which will be discussed in Chapter 3.

2.3. A note on incorporating densities

The above-mentioned continuity equation and equation of motion have been simplified assuming that the densities are $\rho = 1$. Incorporating the density variable ρ as an unknown variable gives a system of equations

$$\begin{cases} \frac{\partial \rho q}{\partial x} + \frac{\partial \rho A}{\partial t} = \rho I \\ \frac{\partial \rho q}{\partial t} + \frac{\partial \rho q v}{\partial x} = \rho g A(S_0 - S_f - S_p) \end{cases} \tag{2.8}$$

Intuitively, incorporating the unknown density variable is desirable in order to add water salinity to the system of equations. However, this adds a complexity to the system of equations since it yields a system with three unknown variables q, A and ρ. Accordingly, both flow velocity, water depths and water salinity would be updated simultaneously yielding complex computational systems with high computational times. Therefore, we will neglect the density variable in the equation of motion. Water salinity is to be incorporated by calculating it in series through adding a third equation to the system; the advection-diffusion equation. Adding this third equation and calculating water salinity is, however, beyond the scope of this thesis.

3

Possible simplifications of the shallow water equations

3.1. General

The full one dimensional shallow water equations describe unsteady nonuniform flow. It describes the water flow in a very detailed manner. Therefore solving the full equations generates high computational costs resulting in an account of turbulent flows on local scales. Instead, for this report we are interested in the general water flow on larger scales. Hence, we wish to look at simplifications of the one dimensional shallow water equations with low computational costs.

In this chapter, possible simplifications of the shallow water equations are outlined. This is done through first introducing different types of flow and subsequently connecting these with a version of the shallow water equations.

3.2. Steady and unsteady flow

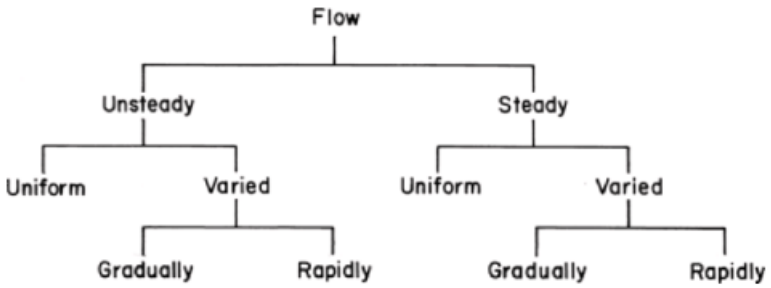

Figure 3.1: Classification of type of flow as illustrated in Fig 1-7 of [6]

Open channel flow is categorized according to steadiness, a condition related to time, and uniformity, a condition related to space. In *steady* open channel flow, the water flow velocity at any point of observation does not change with time, hence it is a stationary process; whereas flow is *unsteady* when the water flow velocity at a specific point changes from moment to moment, which is an instationary process. Open channel flow is

uniform if flow velocity is constant at all points along the channel at all times; whereas flow in *nonuniform*, also called varied, if the flow velocity changes with water moving along the channel. Varied flow is usually subcategorized into gradually varied flow and rapidly varied flow, where the flow varies gradually if the flow velocity varies slowly with respect to distance and the flow varies rapidly if the flow velocity varies significantly over a short distance [5, 6]. More specifically, rapidly varied flow refers to a situation in which changes in depth and velocity occur over short lenghts; considering a scale of a maximum of a couple of meters. Think of flows beneath sluice gates or over weirs. Gradually varied flow refers to a situation in which flow changes in depth and velocity occur over long distances; considering a scale of tens of kilometers [7]. The classification of open channel flow is shown in Figure 3.1 and a graphical representation of the difference between gradually and rapidly varied flow is shown in Figure 3.2.

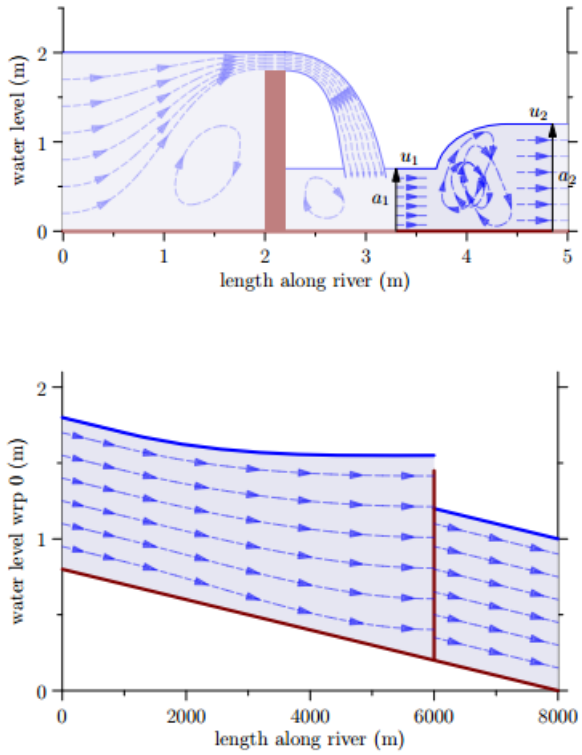

Figure 3.2: Difference in wave behavior around a weir between small and large scales as illustrated in Figure 2.3 and Figure 2.4 in [7]

3.2.1. Steady flow

Uniform flow

Steady flow represents a stationary process, which is a function varying in space and not in time. Thus, for steady flows the time derivative equals zero:

$$\frac{\mathrm{d}v}{\mathrm{d}t} = 0$$

In open channel hydraulics, one usually first considers the stationary process in order to get a general idea of the direction of flow, the variation in flow rate and flow depth along a channel. More specifically, here we start with considering steady uniform flow in which also the spatial derivative equals zero:

$$\frac{\mathrm{d}v}{\mathrm{d}x} = 0$$

Hence, uniform flow in a channel represents a state of dynamic equilibrium. It occurs when the depth of the water, the wetted channel surface area (wetted perimeter) and the flow velocity remain constant in both time and in space, along the channel. Naturally, open channel flow is governed by gravity. The water flow in encounters resistance as it flows down the sloped channel bottom. In a dynamic equilibrium, the gravitational force causing the downflow is equal and opposite to the resistance forces obstructing the flow [10, 11].

Manning's equation describes the relation between friction and flow velocity for steady uniform open channel flow. More specifically, it relates the flow velocity to the hydraulic radius, R, and slope of the channel bed, S_0. It is formulated as

$$v = \frac{1}{n_m} R^{\frac{2}{3}} S_0^{\frac{1}{2}} \tag{3.1}$$

where

v is the average velocity of the water flow (ms^{-1})

n_m is Manning's n, a factor quantifying boundary roughness ($sm^{-\frac{1}{3}}$)

R is the hydraulic radius (m) which is defined by $\frac{A}{P}$; wetted area, A, divided by wetted perimeter, P

S_0 is the channel bed slope or hydraulic gradient (dimensionless)

The n_m in Manning's Equation (3.1) is referred to as the Manning factor n_m or the Gauckler-Manning coefficient, a factor relating the resistance to the roughness of the channel boundaries. It is to be determined empirically. Various studies have been done to provide guidance in choosing appropriate values for n_m . It is common practice to assume that the Gauckler-Manning coefficient n_m is not a function of depth, hence a constant value n_m is considered for a given channel reach [10]. Figure 3.3 shows steady, uniform flow which is an equilibrium situation.

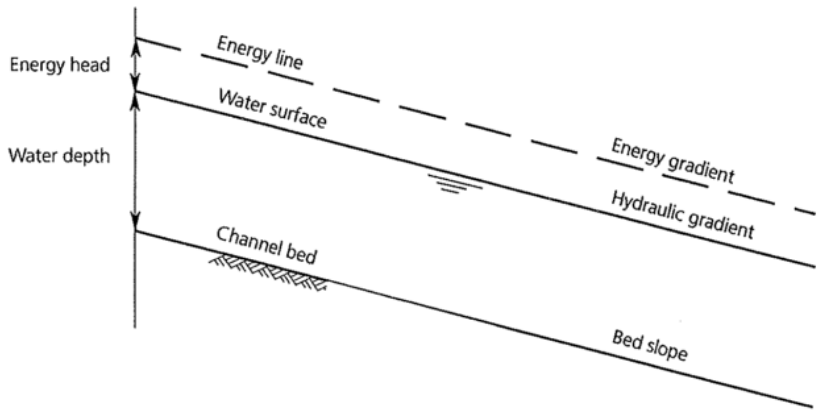

Figure 3.3: As illustrated and stated in Fig 3 of [11]: "Uniform flow considers the water depth, wetted area and velocity constant at each section through the channel. This means that energy line, water surface and channel bed run parallel."

The shallow water equations for steady uniform flow are derived by considering that there is no change in time nor space in the equation of motion (2.6), hence yielding the so-called *kinematic wave model*:

$$\begin{cases} \frac{\partial A}{\partial t} + \frac{\partial q}{\partial x} = I \\ S_0 = S_f \end{cases} \tag{3.2}$$

Nonuniform flow

Similarly, Manning's equation holds for steady nonuniform flow. The only difference being the slope term; namely, S_f is considered instead of S_0. S_f is the total energy gradient which is the the slope of the total energy line. In uniform flow the energy gradient equals the channel bed slope. However, this is not the case in nonuniform flow since the flow velocity changes along the channel [6, 10]. Accordingly, Manning's equation becomes

$$v = \frac{1}{n_m} R^{\frac{2}{3}} S_f^{\frac{1}{2}} \tag{3.3}$$

which can also be rewritten, using $A = qv$, as

$$S_f = \frac{n^2 q|q|}{A^2 R^{2/3}} \tag{3.4}$$

Two possible simplifications of the shallow water equations for steady nonuniform flow are the *steady dynamic wave model* and the *diffusion wave model*. The latter has been found to be a more accurate approximation of the full shallow water equations [9]. The steady dynamic wave model is given by

$$\begin{cases} \frac{\partial q}{\partial x} + \frac{\partial A}{\partial t} = I \\ \frac{\partial qv}{\partial x} = gA(S_0 - S_f - S_p) \end{cases} \tag{3.5}$$

and the diffusion wave model is given by

$$\begin{cases} \frac{\partial q}{\partial x} + \frac{\partial A}{\partial t} = I \\ S_p = S_0 - S_f \end{cases} \tag{3.6}$$

The diffusion wave type of flow is illustrated in the second picture in Figure 3.2.

3.2.2. Unsteady flow

In unsteady open channel flow, flow velocities and depths change with time at any fixed spatial position in the channel. Naturally, open channel flow in channels is unsteady and nonuniform because of the free surface. Mathematically, this means that the two dependent flow variables, velocity and depth, are functions of both distance x along the channel and time t. Mathematical problem formulation requires two partial differential equations representing the continuity and momentum principles in the two unknown dependent variables [5]. Hence, this is modeled by the full shallow water equations 2.1 which are also referred to as the *dynamic wave model*.

3.3. Our model requirements

In this thesis report, three of the above-mentioned models will be explored; namely, the kinematic wave model, the diffusion wave model and the dynamic wave model. The kinematic wave is a logical starting point as a main focus of this research for a fast and simple water flow model. It models steady and uniform flow. Hence, it neglects the short and local waves occurring around weirs and sluice gates. The diffusion and dynamic wave models will also be explored to enable a comparison with the kinematic wave.

4

Testing the kinematic wave model

4.1. The kinematic wave model

As a starting point for this research, we have chosen to focus on the kinematic wave model which is a simplified version of the shallow water equations. The kinematic wave model is given by

$$\begin{cases} \frac{\partial A}{\partial t} + \frac{\partial q}{\partial x} = I \\ S_0 = S_f \end{cases} \tag{4.1}$$

where q is discharge, A is the cross sectional area, I is the external in- or outflow, S_0 is the channel bed slope and S_f is the friction slope. The following paragraphs will discuss the interpretation and solution methods for the kinematic wave equation.

4.1.1. Interpretation and assumptions

Similarly to the shallow water equations, we assume hydrostatic pressure in the kinematic wave model. Also, the friction slope S_f is determined with the empirical equations formulated by Manning, as discussed in Section 3.2.1.

Specifically in the kinematic wave model, the water wave is assumed to be long and flat so that S_f almost equals the channel bed slope S_0. Hence the *local acceleration* term $\frac{\partial q}{\partial t}$, the *convective acceleration* term $\frac{\partial A}{\partial x}$ term and the pressure force term S_p in the equation of motion (2.6) all disappear. Thus, the channel bed slope S_0 is assumed to be large enough and the water wave long and flat enough so that all the other terms in the equation of motion are negligible. Accordingly, a kinematic wave is described by the continuity equation together with a uniform flow equation, such as Manning's equation. It describes a steady and uniform flow within each differential length [8].

In addition, the discharge q is assumed to be a function of the water depth alone; so each wave travels with constant wave speed along the channel. This wave speed, also called wave celerity, is given by $c = \frac{\partial q}{\partial A}$. As a result, kinematic waves only propagate downstream and do not attenuate as they propagate downstream [9]

4.1.2. The kinematic wave equation

The kinematic wave model (4.1) consists of the continuity equation

$$B\frac{\partial h}{\partial t}+\frac{\partial q}{\partial x}=I \tag{4.2}$$

together with the equation of motion in its simplified version of steady uniform flow; namely,

$$S_0=S_f \tag{4.3}$$

With Manning's equation (3.1), assuming a perpendicular channel such that the cross sectional area is given by $A=Bh$ with fixed B, using the definition of discharge $q=Av$ and the definition of the hydraulic radius $R=A/P$ which in this case is $R=Bh/(2h+B)$, equation (4.3) can be expressed in the form

$$q=\frac{1}{n_m}S_0^{1/2}\frac{(Bh)^{5/3}}{(2h+B)^{2/3}} \tag{4.4}$$

By differentiating (4.4) with respect to x

$$\frac{\partial q}{\partial x}=\frac{1}{n_m}S_0^{1/2}B^{5/3}\frac{\partial}{\partial x}\left(\frac{h^{5/3}}{(2h+B)^{2/3}}\right) \tag{4.5}$$

and plugging the resulting expression (4.5) into equation (4.2) whilst setting the coefficient $\alpha=\frac{1}{n_m}S_0^{1/2}B^{2/3}$, one arrives at the kinematic wave equation in terms of the water depth h

$$\boxed{\frac{\partial h}{\partial t}+\alpha\frac{\partial}{\partial x}\left(\frac{h^{5/3}}{(2h+B)^{2/3}}\right)=\frac{1}{B}I} \tag{4.6}$$

4.2. Analytical solution of the kinematic wave equation

The kinematic wave equation is a first-order nonlinear hyperbolic partial differential equation (PDE). The solution can be obtained analytically in simple cases. Although the main focus of this thesis is on obtaining the numerical solution, the analytical solution is given as well to set the framework.

The analytical solution of the kinematic wave equation is obtained by the method of characteristics. Characteristic curves for a PDE are curves along which the equation simplifies [12]. The characteristic equations for the kinematic wave are two ordinary differential equations which are mathematically equivalent to the continuity and momentum equation [8, 13], given by

$$\begin{cases}\frac{\mathrm{d}h}{\mathrm{d}t}=I\\ c=\frac{1}{B}\frac{\mathrm{d}q}{\mathrm{d}h}\end{cases} \tag{4.7}$$

where the second equation in (4.7) for the wave celerity can be rewritten as follows

$$\frac{\mathrm{d}x}{\mathrm{d}t}=\frac{1}{B}\frac{\mathrm{d}q}{\mathrm{d}h}=\alpha\frac{\mathrm{d}}{\mathrm{d}h}\left(\frac{h^{5/3}}{(2h+B)^{2/3}}\right)=\alpha\frac{h^{2/3}(6h+5B)}{3(2h+B)^{5/3}} \tag{4.8}$$

Along these curves the solution is constant and traveling with finite propagation speed. Hence, solving these

gives the analytical solution, with $h = \int_{t_0}^{t} I\,\mathrm{d}t + h_0$ following from the first equation in (4.7),

$$x - x_0 = \alpha \int_{t_0}^{t} \left[\frac{5h^{2/3}}{(2h+B)^{2/3}} - \frac{4h^{5/3}}{(2h+B)^{5/3}} \right] \mathrm{d}t \tag{4.9}$$

4.3. Numerical solution of the kinematic wave equation

The solution of the kinematic wave can be obtained numerically using finite difference or finite volume methods. In this thesis, the focus will be on solving the PDEs using finite volume methods since these are exactly conservative and also more robust in presence of discontinuities [12]. In this section, the build up to the numerical method is outlined. Firstly, the numerical solution method to a scalar linear hyperbolic PDE is derived so that the numerical solution methods for the nonlinear kinematic wave equation follow easily.

4.3.1. Initial solution and boundary conditions

Before diving into the derivation of numerical approximation methods, it is important to make two remarks. First of all, in order to apply any numerical approximation method to solve an equation, an initial guess of the solution has to be made. This initial guess represents the values of the solution at the first time step t_0. From there, the solution of the equation can be approximated numerically for the following time steps.

Second of all, the boundary values of a numerical method always need some special care. The boundaries of a numerical method are the beginning and end points. Estimating the values for these boundaries is tricky because there is only one neighboring point, instead of two neighboring points, to which the numerical method can be applied. Therefore, the boundary values are defined separately. For testing numerical methods, the easiest approach to defining these boundary values is by using periodic boundary conditions. In periodic boundary conditions, the end points values are again used as the beginning points values. Clearly, periodic boundary conditions are not applicable for water flow in a ditch in a Dutch polder network. Therefore, Dirichlet boundary conditions are used for the test cases. How these periodic and the Dirichlet boundary conditions were defined precisely will be explained later.

4.3.2. Numerical approximation of the advection equation

The kinematic wave equation is a scalar nonlinear hyperbolic equation which belongs to the class of conservation laws. A conservation law takes the form

$$w_t(x,t) + f(w(x,t))_x = \Psi(w(x,t),x,t) \tag{4.10}$$

where $f(w)$ is the flux function which governs the fluxes in and out of the finite volumes and $\Psi(w(x,t),x,t)$ is the source function which accounts for external effects that change the quantity of interest. First, a linear equation is considered; namely, the advection equation in scalar form. The advection equation describes a substance being carried along by fluid motion at constant velocity $\bar{u}$ in which the concentration w of the substance is given by

$$w_t(x,t) + \bar{u} w_x(t,x) = 0 \tag{4.11}$$

This is a linear hyperbolic equation, also belonging to the class of conservation laws. Here, a numerical approximation method for the advection equation is derived and verified so that subsequently a numerical approximation method for the nonlinear kinematic wave equation can be developed. The nonlinear method is build further upon the linear approximation method.

Finite volume methods are based on the integral form of the conservation law. The spatial domain is

divided into intervals, the finite volumes. For each of these finite volumes, the average of w over the volume is approximated. In each time step, these values are updated using approximations to the fluxes in and out of each finite volume. Obtaining the solution requires an initial condition of concentrations $w(x,0)$ specified at all points in the domain. In addition, an upstream boundary condition $w(0,t)$ needs to be specified.

The finite volume method as illustrated in Léveque will be employed to derive a numerical approximation method for the advection equation [12]. Let's first consider a channel of length L and assume that the external in- and outflows are negligible, so the source term $\Psi(w(x,t),x,t)=0$. Accordingly, the channel is subdivided into N finite volumes, in this case simply N intervals. Define the ith interval by

$$\mathcal{C}_i = (x_{i-1/2}, x_{i+1/2})$$

for $i = 1,...,N$. Consider the well known finite difference approach to the general conservation law (4.10) with $\Psi = 0$ given by

$$\frac{W_i^{n+1} - W_i^n}{\Delta t} + \frac{F_{i+1/2}^n - F_{i-1/2}^n}{\Delta x} = 0 \tag{4.12}$$

where Δx is the length of the finite volume interval, Δt the length of the time step, W_i^n corresponds to the average value of the concentration w in the interval $\mathcal{C}_i$ for $i \in 1,...,N$ at time $n \in 1,...,t_{end}$, $F_{i-1/2}^n$ to the flux on the right hand side of interval $\mathcal{C}_i$ and $F_{i+1/2}^n$ to the flux on the left hand side of interval $\mathcal{C}_i$ as shown in Figure 4.1.

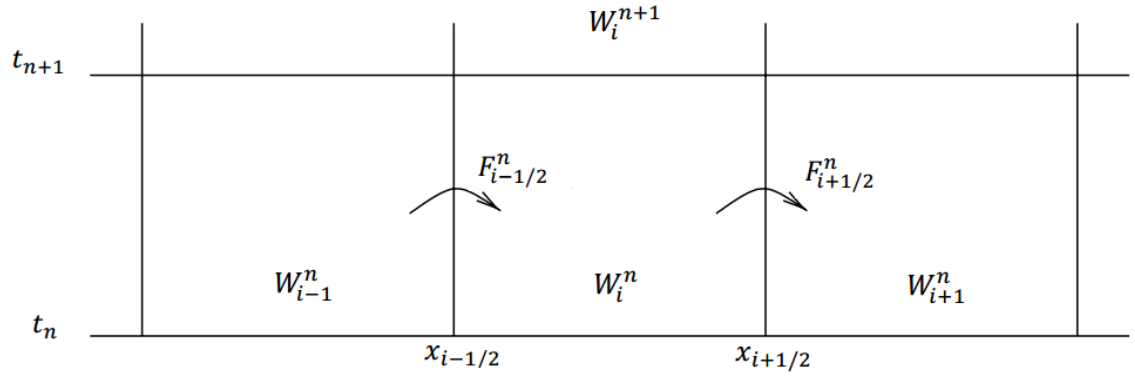

Figure 4.1: Finite volume grid adapted from [12]

In the finite volume method, the value W_i^n at the interval $\mathcal{C}_i$ is obtained by integrating over the concentration w for each interval as given by

$$W_i^n \approx \frac{1}{\Delta x}\int_{x_{i-1/2}}^{x_{i+1/2}} w(x,t_n)\mathrm{d}x \tag{4.13}$$

Therefore, the finite volume method averages the concentration function $w(x,t)$. Hence resulting in a conservative numerical method. In comparison, for a finite difference method one would choose to consider the pointwise value

$$w_i^n = w(x_i, t_n) \tag{4.14}$$

at the interval $\mathcal{C}_i$ instead of the average value W_i^n as in equation (4.13).

Note that the pointwise value (4.14) at the cell center x_i agrees with the cell average (4.13) up to an accuracy of order $\mathcal{O}(\Delta x^2)$ for sufficiently smooth functions $w(x,t)$. The finite volume methods applied in this thesis are either of order $\mathcal{O}(\Delta x)$ or order $\mathcal{O}(\Delta x^2)$. Thus, the error resulting from taking the pointwise value, instead of the average value, is negligible. Accordingly, in this thesis the pointwise values will be used for simplicity.

In addition, $F^n_{i-1/2}$ in equation (4.12) is an approximation of the average flux at point $x_{i-1/2}$

$$F^n_{i-1/2} \approx \frac{1}{\Delta t}\int_{t_n}^{t_{n+1}} f(w(x_{i-1/2},t))\mathrm{d}t \tag{4.15}$$

where the above integral can be approximated using different possible numerical flux functions $\mathcal{F}$ such that

$$F^n_{i-1/2} = \mathcal{F}(W^n_{i-1}, W^n_i)$$

Accordingly, the finite volume method for conservation laws, and in this case for the kinematic wave equation, can be rewritten in the finite volume form as

$$W^{n+1}_i = W^n_i - \frac{\Delta t}{\Delta x}\left[\mathcal{F}(W^n_i, W^n_{i+1}) - \mathcal{F}(W^n_{i-1}, W^n_i)\right] \tag{4.16}$$

In this thesis, two different flux methods are considered that define the average fluxes $F^n_{i-1/2}$ in different ways; namely, the Upwind method and the Lax-Wendroff method.

Upwind method The Upwind method is of first order accuracy and introduces the most numerical diffusion yielding smeared results compared to the Lax-Wendroff method. However, it is the easiest to compute. The flux functions determine the fluxes in and out of a finite volume cell. Therefore, the cell average is affected by the net change in flux in a cell.

To quantify this flux, think of the jump $\mathcal{W}_{i-1/2} = W^n_i - W^n_{i-1}$ as a wave traveling into cell $\mathcal{C}_i$ with positive velocity λ^+ and $\mathcal{W}_{i+1/2} = W^n_{i+1} - W^n_i$ with negative velocity λ^- where

$$\lambda^+ = \max(\lambda, 0), \qquad \lambda^- = \min(\lambda, 0) \tag{4.17}$$

In this scalar advection case, λ is the eigenvalue that results from the constant coefficient $\bar{u}$ in the flux term

$$\bar{u}\, w_x(x,t)$$

in the conservation equation (4.11). Trivially, the eigenvalue of $\bar{u}$ equals $\lambda = \bar{u}$. In the case of a linear system of two equations, there is a constant coefficient matrix $A \in \mathbf{R}^{2\times 2}$ with two eigenvalues corresponding to two different wave velocities.

Now, the cell average in cell $\mathcal{C}_i$ is affected by all the right-going waves from $x_{i-1/2}$ and all the left-going waves from $x_{i+1/2}$. In case of a scalar equation, there is simply one wave either traveling to the right or to the left. Accordingly, the Upwind fluxes are given by

$$F^n_{i+1/2} = \lambda^-(W^n_{i+1} - W^n_i)$$
$$F^n_{i-1/2} = \lambda^+(W^n_i - W^n_{i-1})$$

Note that in the scalar advection case, one of these fluxes disappears since there is only one wave velocity λ which is either positive or negative. The procedure described above is illustrated in Figure 4.2.

With above expressions for the Upwind fluxes, the Upwind method for the scalar advection equation, resulting from equation (4.16), is given by

$$W^{n+1}_i = W^n_i - \frac{\Delta t}{\Delta x}(\lambda^-(W^n_{i+1} - W^n_i) - \lambda^+(W^n_i - W^n_{i-1})) \tag{4.18}$$

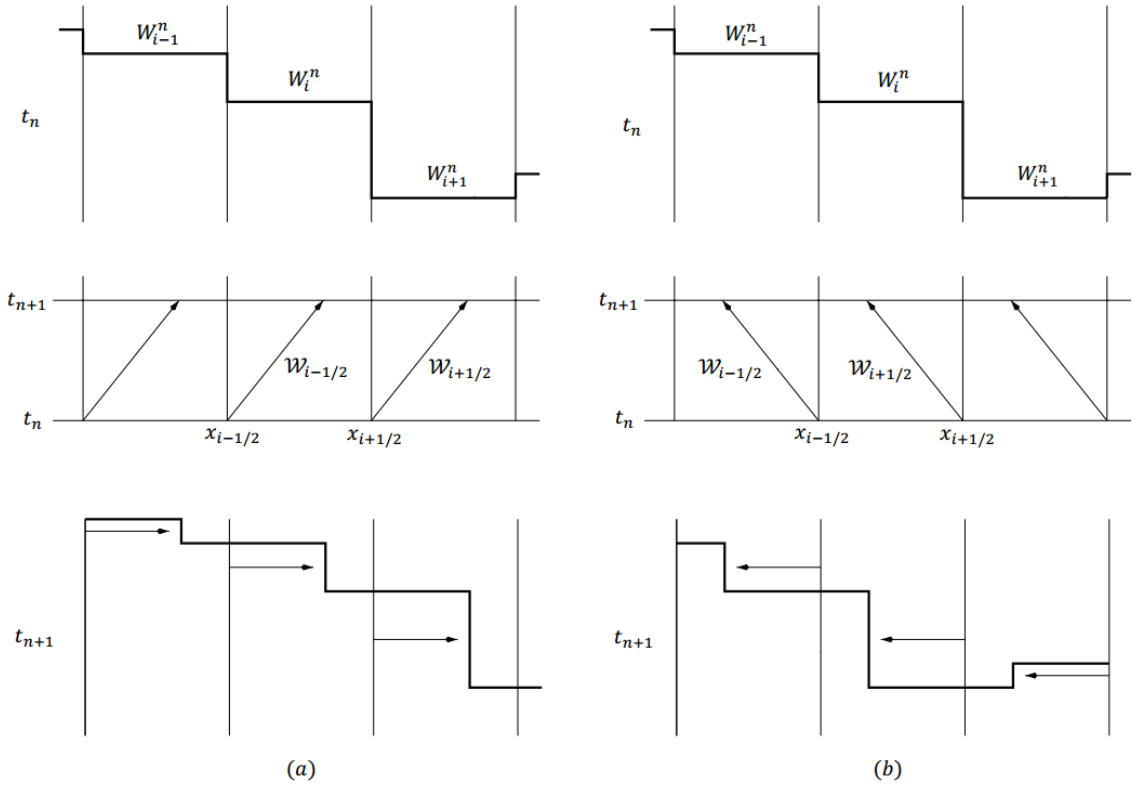

Figure 4.2: The Upwind method for the scalar advection equation illustrated by a wave-propagation interpretation, adapted from [12]. The top graphs show the data at time t_n. The discontinuities at $x_{i-1/2}$ and $x_{i+1/2}$ are seen as the waves $\mathcal{W}_{i-1/2}$ and $\mathcal{W}_{i+1/2}$ respectively. Over time Δt, these waves propagate with speed $\bar{u}$, hence shifting a distance of $\bar{u}\Delta t$ which is shown in the middle graphs where $\bar{u} > 0$ in graphs (a) and $\bar{u} < 0$ in graphs (b). The new positions of the waves at time t_{n+1} are shown in the bottom graphs. The new cell averages are then computed by averaging the function in each cell.

The Upwind method for the advection equation was implemented and tested on initial data given in the book by Leveque [12]. In order to do so, periodic boundary conditions were considered and the CFL condition was taken to be 0.8. Periodic boundary conditions means that

$$W_0^n = W_N^n, \quad W_{N+1}^n = W_1^n$$

at each time step. The CFL condition will be discussed in Section 4.3.4. Figure 4.3 shows the result.

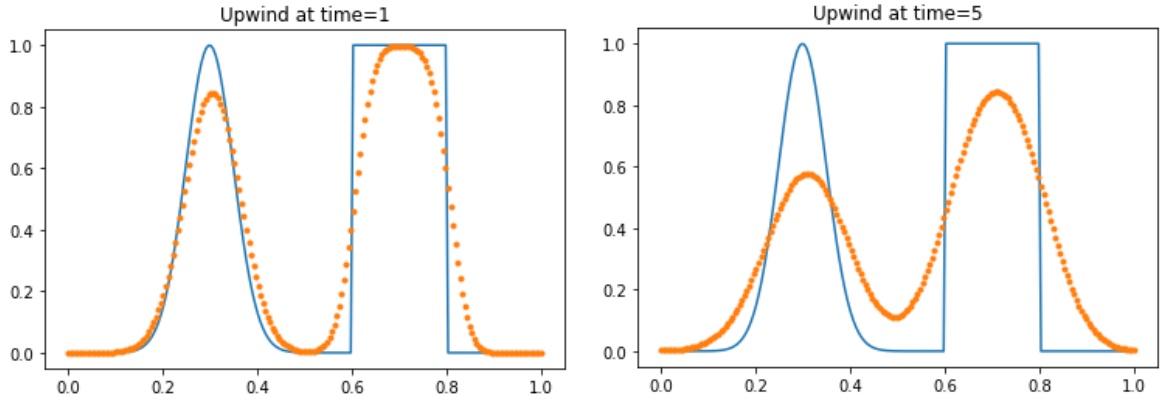

Figure 4.3: The Upwind method for the advection equation implemented and verified using the results in the book by LeVeque [12]. The blue function is showing the initial data and the orange dots correspond to the upwind computed solution.

Lax-Wendroff method The Lax-Wendroff method is a centered three point method. It is based on the Taylor series expansion and is of second order accuracy. This method is able to capture wave behavior better in comparison to the Upwind method. However, the error in the Lax-Wendroff method results from the dispersive term, $w_{ttt} = -\bar{u}^3 w_{xxx}$, which causes oscillatory behavior in the solution, see pages 100-102 and 154 in [12].

The Upwind method yielded the formula (4.16), which is the simplest finite volume method. In order to gain more accuracy in the finite volume method, the following general formula is introduced;

$$W_i^{n+1} = W_i^n - \frac{\Delta t}{\Delta x}(\lambda^-(W_{i+1}^n - W_i^n) - \lambda^+(W_i^n - W_{i-1}^n)) - \frac{\Delta t}{\Delta x}(\tilde{F}_{i+1/2} - \tilde{F}_{i-1/2}) \tag{4.19}$$

in which $\tilde{F}_{i+1/2}$ and $\tilde{F}_{i-1/2}$ are correction terms which are defined depending on the method. For the linear Lax-Wendroff method in scalar form, $\tilde{F}_{i-1/2}$ is defined as

$$\tilde{F}_{i-1/2} = \frac{1}{2}|\lambda|(1 - \frac{\Delta t}{\Delta x}|\lambda|)(W_i^n - W_{i-1}^n) \tag{4.20}$$

The Lax-Wendroff method for the advection equation was implemented in a similar manner as was done for the Upwind method. The result is shown in Figure 4.4.

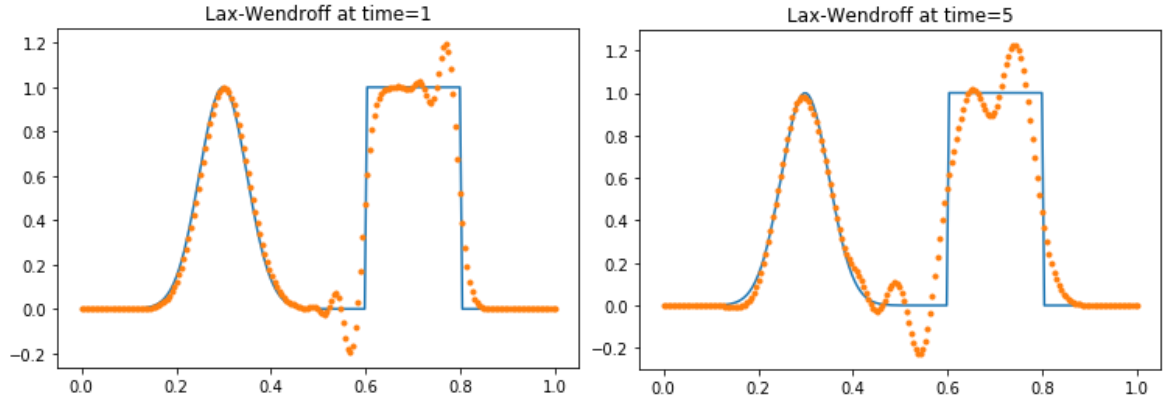

Figure 4.4: The Lax-Wendroff method for the advection equation implemented and verified using the results in the book by LeVeque [12]. The blue function is showing the initial data and the orange dots correspond to the Lax-Wendroff computed solution.

4.3.3. Numerical approximation of the kinematic wave equation

The kinematic wave equation (4.1) is a nonlinear conservation law of the form

$$h_t(x,t) + f(h(x,t))_x = \Psi(h(x,t),x,t) \tag{4.21}$$

where $f(h)$ is the flux function which governs the fluxes in and out of the finite volumes and $\Psi(h(x,t),x,t)$ is the source function which accounts for external effects that change the quantity of interest in addition to the fluxes. Specifically, the flux function for the kinematic wave equation is $f(h(x,t)) = \frac{h^{5/3}}{(2h+B)^{2/3}}$ and the source function $\Psi(h(x,t),x,t) = I(h(x,t),x,t)$ accounts for external in- or outflows. The nonlinearity results from the nonlinear flux function f. The finite volume solution method for scalar nonlinear equations is an extension of the finite volume method for linear equations described for the advection equation in the previous section. Note that obtaining a solution requires an initial condition of depths $h(x,0)$ specified at all points of the water channel, which can also be rewritten into discharge $q(x,0)$ using equation (4.4). In addition, an upstream boundary condition $h(0,t)$ or $q(0,t)$ needs to be specified.

For the nonlinear case, the solution again yields a set of waves $\mathcal{W}_{i-1/2} \in \mathbb{R}$ for $i \in 1,...,N$, but now with wavespeeds $s_{i-1/2} \in \mathbb{R}$ which are varying per grid cell $\mathcal{C}_i$. The wavespeeds $s_{i-1/2}$ are defined using the Rankine-Hugoniot shock speed

$$s_{i-1/2} = \begin{cases} [f(H_i) - f(H_{i-1})]/(H_i - H_{i-1}) \\ f'(H_i) \end{cases} \tag{4.22}$$

where $H_i \approx \frac{1}{\Delta x}\int_{x_{i-1/2}}^{x_{i+1/2}} h(x,t_n)\mathrm{d}x$. The nonlinear flux functions become

$$F^n_{i+1/2} = (s_{i+1/2})^-(H^n_{i+1} - H^n_i)$$
$$F^n_{i-1/2} = (s_{i-1/2})^+(H^n_i - H^n_{i-1})$$

Accordingly, the Upwind method becomes

$$H^{n+1}_i = H^n_i - \frac{\Delta t}{\Delta x}[(s_{i+1/2})^-(H^n_{i+1} - H^n_i) - (s_{i-1/2})^+(H^n_i - H^n_{i-1})] \tag{4.23}$$

which can be expanded with the Lax-Wendroff flux correction terms, written as

$$\tilde{F}_{i-1/2} = \frac{1}{2}|s_{i-1/2}|(1 - \frac{\Delta t}{\Delta x}|s_{i-1/2}|)(H^n_i - H^n_{i-1}) \tag{4.24}$$

Finally, the source term $\Psi(h(x,t),x,t) = \frac{1}{B}I(x,t)$ is to be implemented in the finite volume method. For this, the fractional step method is employed. The kinematic wave equation is separated into two problems

$$\text{Problem A: } h_t + \left(\frac{h^{5/3}}{(2h+B)^{2/3}}\right)_x = 0 \tag{4.25}$$

$$\text{Problem B: } h_t = I(h(x,t),x,t) \tag{4.26}$$

resulting in the following procedure. In the first step, the Upwind method or the Lax-Wendroff method is applied. The Upwind method is considered in the example below. In the second step, the forward Euler for

the ODE of problem B is applied. Accordingly,

$$\text{A-step: } H_i^* = H_i^n - \frac{\Delta t}{\Delta x}[(s_{i+1/2})^-(H_{i+1}^n - H_i^n) - (s_{i-1/2})^+(H_i^n - H_{i-1}^n)] \tag{4.27}$$

$$\text{B-step: } H_i^{n+1} = H_i^* + \Delta t \frac{1}{B} I \tag{4.28}$$

which can be rewritten by eliminating H_i^* as follows

$$H_i^{n+1} = H_i^n - \frac{\Delta t}{\Delta x}[(s_{i+1/2})^-(H_{i+1}^n - H_i^n) - (s_{i-1/2})^+(H_i^n - H_{i-1}^n)] + \Delta t \frac{1}{B} I \tag{4.29}$$

4.3.4. Necessary and sufficient conditions for convergence

An important requirement for a numerical method is convergence, meaning that the numerical solution should converge to the true solution of the differential equation as the grid is refined when $\Delta x \to 0$ and $\Delta t \to 0$. Convergence of a method requires it to be both *consistent* and *stable*. In addition, we require positive water depths h everywhere on the grid to prevent breaking of the flux functions.

Consistence A numerical method is consistent with the differential equation if it approximates the true solution well locally. More specifically, it is consistent if the local truncation error vanishes as $\Delta x, \Delta t \to 0$ for all smooth functions satisfying the differential equation under consideration. The local truncation error is defined by

$$\tau^n = \frac{1}{\Delta t}[\mathcal{N}(h^n) - h^{n+1}] \tag{4.30}$$

in which $\mathcal{N}(\cdot)$ is the numerical operator mapping the approximate solution at time n to the approximate solution at time $n+1$ for $n = 1, ..., t_{end}$ so that the one-step-error is defined by

$$\mathcal{N}(h^n) - h^{n+1}$$

and from which the definition of the truncation error follows naturally. For scalar linear methods, such as the advection equation, the truncation error indeed vanishes with $\Delta x, \Delta t \to 0$ for the Upwind and Lax-Wendroff method, see page 142-143 in Leveque [12]. For nonlinear scalar methods, such as the kinematic wave equation, it is more complicated as there is no constant wavespeed and the local truncation error needs to be checked for every wavespeed $s_{i+1/2}^-$ and $s_{i-1/2}^-$.

Stability Stability of a method requires local truncation errors to not grow rapidly. Hence, to show stability, a bound on the global error can be obtained using the local truncation errors. Leveque outlines the approach of showing stability for the Upwind and Lax-Wendroff method for the advection equation on pages 145-148 [12].

The CFL condition: a necessary condition for stability Very important is the notion of the Courant-Friedrichs-Lewy (CFL) condition as a necessary condition condition for stability and thus convergence. It is, however, not a sufficient condition. The CFL condition is stated by Leveque [12]: "A numerical method can be convergent only if its numerical domain of dependence contains the true domain of dependence of the PDE, at least in the limit as Δt and Δx go to zero". To illustrate this, consider Figure 4.5

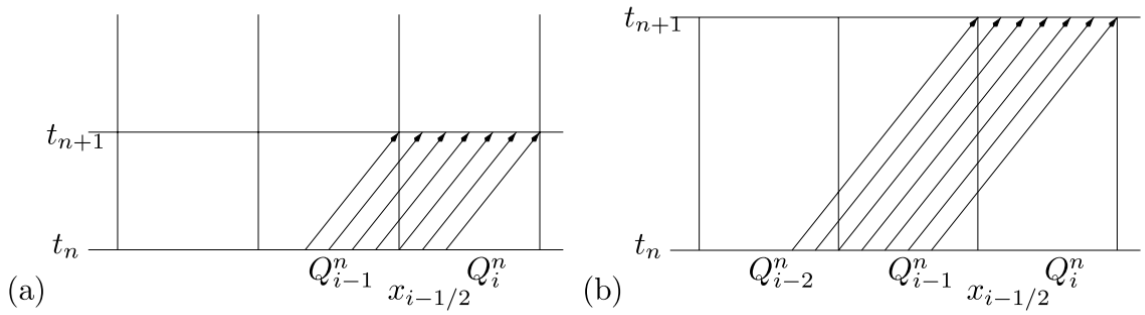

Figure 4.5: The CFL condition

Figure 4.5 shows the characteristic curves of the advection equation for two different time step lengths. Considering explicit methods, such as the Upwind method or the Lax-Wendroff method, the computation of H_i^{n+1} depends on the values in three grid cells H_{i-1}^n, H_i^n and H_{i+1}^n. For the small time step shown in Figure 4.5.a this works well; namely, the characteristic curves at time $n+1$ in cell H_i only depend on cells H_{i-1} and H_i from time step n. However, it is going wrong in 4.5.b; the characteristic curves at time $n+1$ in cell H_i now also depend on cells H_{i-2}. This gives a problem because the explicit methods discussed here do not incorporate H_{i-2} in computation of the value for H_i in the next time step $n+1$. Thus, there is some missing information. This problem causes for instability issues. Therefore, it is very important to choose the spatial and time discretization steps properly.

For the linear advection equation, this means that the following bound holds:

$$|\frac{\bar{u}\Delta t}{\Delta x}| \leq 1 \tag{4.31}$$

For the nonlinear kinematic wave equation, this leads to the following bound:

$$\frac{\Delta t}{\Delta x}\max|f'(h)| \leq \frac{1}{2} \tag{4.32}$$

for every value of $h = H_i$ arising in the computations.

4.4. Verification of the developed numerical methods

The developed numerical methods for the advection equation in Section 4.3.2 and for the kinematic wave equation in Section 4.3.3 need to be verified. Verification can be done by comparison to analytical solutions or to the solutions found in the literature. This is possible for the advection equation by comparing it to Leveques results [12]. However, analytical results or literature results for these numerical methods for the kinematic wave equation are not available. Therefore, the method of manufactured solutions is applied to both the advection equation and the kinematic wave equation.

4.4.1. Method of manufactured solutions (MMS)

The method of manufactured solutions works as follows: first, a feasible solution to the equation is assumed and plugged into the equation. Accordingly, the source term, boundary term and the initial value term can be derived. Then the numerical method is applied using these three terms. If all is well, the assumed solution should result from the application of the in Sections 4.3.2 and 4.3.3 developed numerical methods.

4.4.2. MMS for the advection equation

Consider the advection equation assuming the wave speed $\bar{u} = 1$

$$w_t + w_x = 0 \tag{4.33}$$

and assuming the solution $w(x,t) = -\sin(t-x)$. Accordingly, the boundary $x = 0$ has the value $w(0,t) = -\sin(t)$ and the initial condition at $t = 0$ has the value $w(x,0) = \sin(x)$. Comparing the solution $w(x,t) = -\sin(t-x)$ with the numerical results when the Upwind method and the Lax-Wendroff method are applied with the boundary condition $w(0,t) = -\sin(t)$ and initial condition $w(x,0) = \sin(x)$, results in small differences between the real solution and the numerically computed solution as is shown in Table A.1 and Table A.2. Thus, the developed Upwind and Lax-Wendroff numerical methods are verified.

4.4.3. MMS for the kinematic wave equation

For the kinematic wave equation, the method of manufactured solutions works similarly as described above for the advection equation. Additionally, there is a source term $\Psi(x,t) = I(t,x)$. Suppose the solution is $h(x,t) = \sin(x-t) + \frac{3}{2}$ which has to be positive everywhere because depths h cannot be negative. Plugging this assumed solution into the kinematic wave equation (4.1), assuming that the channel width $B = 1$ and the constant $\alpha = 1$, yields the boundary condition $h(0,t) = -\sin(t) + \frac{3}{2}$, the initial condition $h(x,0) = \sin(x) + \frac{3}{2}$ and a source term defined by

$$I(x,t) = -\cos(t-x) + \frac{5}{3}\frac{\cos(t-x)(\frac{3}{2} - \sin(t-x))^{2/3}}{(1+2(\frac{3}{2} - \sin(t-x))^{2/3}} - \frac{4}{3}\frac{\cos(t-x)(\frac{3}{2} - \sin(t-x)^{5/3}}{(1+2(\frac{3}{2} - \sin(t-x)))^{5/3}}$$

To test the numerical methods, the number of intervals was set to $nx = 24$, with the interval distance $\Delta x = \frac{2\pi}{24} \approx 0.26$ and the time step $\Delta t = \frac{1}{2}\Delta x \approx 0.19$ which gives that $dt \approx 0.8dx$ so that the CFL number is approximately 0.467 which is close to the CFL number limit of $\frac{1}{2}$. Finding the accuracy of the kinematic wave equation was done by applying the Richardson extrapolation method mentioned on page 34 in [14]. Thus, $\frac{\Delta x}{2}$, $\frac{\Delta t}{2}$ and $\frac{\Delta x}{4}$, $\frac{\Delta t}{4}$ were evaluated to find the behavior of the error between the assumed solution $h(x,t)$ and the computed solution $H(x,t)$ for both the Upwind and the Lax-Wendroff method. For this, an end time of 60 minutes was considered.

Theoretically, the error between the assumed solution $h(x,t) = \sin(x-t) + \frac{3}{2}$ and the Upwind numerical solution is of the order $\mathcal{O}(\Delta x)$. For the Lax-Wendroff method, the error is of the order $\mathcal{O}((\Delta x)^2)$ theoretically. To test this in practice, a method is of first order accuracy if the error is halved when both the spatial discretization step and the time step are halved. It is of second order accuracy when the error becomes a quarter for halving the discretization step and time step. Tables A.3 and A.4 in the Appendix show the results of these computations. They both show that the errors are roughly halving for halving discretization steps, hence both methods seem to be of first order accuracy as implemented in this thesis.

4.5. Implementation

The developed finite volume methods for the kinematic wave are applied to the scenario of a straight ditch in a Dutch polder network. A ditch of length 1 km, width 1 m and a downstream depth of 1 m is considered. The value for the Gauckler-Manning coefficient is set to $n_m = 0.04$ which represents a channel with some friction caused by weeds and stones.

4.5.1. Initial solution and boundary conditions

Initial solution To be able to apply the numerical method, an initial solution needs to be specified everywhere in the computational domain. Here, the computational domain is simply the straight ditch. Generally, the initial solution $h(x,0)$ is specified everywhere in the ditch to equal the downstream water depth, imitating a flat water level along the ditch [15]. However, various initial solutions are implemented in this section to test and show the results of the finite volume methods for the kinematic wave.

Boundary conditions The finite volume method is in practice applied to a finite domain. Hence, there is no information for the values of the neighboring cells in the first and the last interval. Therefore, one needs boundary conditions specifying the necessary information for applying the finite volume method on the boundary intervals. Depending on the chosen flux method, one either needs one or two ghost cells on the boundaries. A ghost cell is an interval outside of the computational domain to which hypothetical values are assigned to enable the computation of the numerical method on the boundary intervals. Let's consider the interval $[a,b]$ where $x=a$ is the left boundary and $x=b$ the right boundary.

Inflow boundary

The inflow ghost cell values could be assigned using knowledge of the characteristic equations [12]. However, the kinematic wave equation is a nonlinear equation for which the characteristic equations are not immediately known. Instead, a Dirichlet boundary condition is implemented on the inflow boundary which specifies a given value or function at the location $x=a$, for example $q(a,t)=50$ which can be transformed into a depth H_0^n for all time steps n using equation (4.4). It follows that there are no ghost cells needed on the inflow boundary.

Outflow boundary

The outflow boundary values do not always need to be specified depending on the chosen flux method. Only if the flux method needs the next interval for computation, such as in the Lax-Wendroff method, then the outflow boundary should be specified and either one or two ghost cells are necessary. The simplest way of assigning these ghost values is to use zero-order extrapolation, which is simply assigning the ghost cells values of a constant function [12]. Hence,

$$H_{N+1}^n = H_N^n, \quad H_{N+2}^n = H_N^n \tag{4.34}$$

4.5.2. Results

No external inflow The flow behavior of a water pulse was investigated for the case of zero external inflows. The results of the tests on the pulse behavior showed that when there is no channel bed slope, the kinematic wave model does not model any water flow. This is because kinematic wave motion is solely based on gravitational forces resulting from the difference in channel bed heights. To illustrate this, three different cases were implemented for the pulse. In all these test cases the ditch is set to be of length 1 km, width 1 m, with a Gauckler-Manning coefficient of $n_m = 0.04$. The Dirichlet upstream boundary condition is in all cases set to a depth of 1 meter, corresponding to a fixed inflow discharge depending on the channel bed slope.

Firstly, a zero channel bed slope ditch was assumed. Figure 4.6 shows the resulting water depths along the ditch for both the Upwind and the Lax-Wendroff method. Clearly, in this case the water pulse does not move due to the zero channel bed slope. Here the inflow discharge is $q = 0\ m^3/s$.

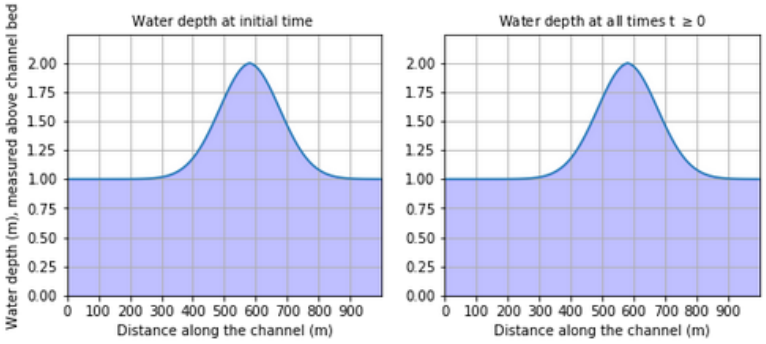

Figure 4.6: A pulse in a ditch with zero channel bed slope, so $S_0 = 0$. Hence, resulting in zero water flow at all times.

Secondly, the Upwind method was applied to the pulse in a ditch with a channel bed slope of 1 meter per kilometer. The inflow discharge is $q(0,t) = 0.38\, m^3/s$. The water starts moving. Figure 4.7 shows the pulse at the initial time and two later times. It was not plotted that he final situation, for times $t \geq 30$, is a ditch with a water depth of 1 meter everywhere.

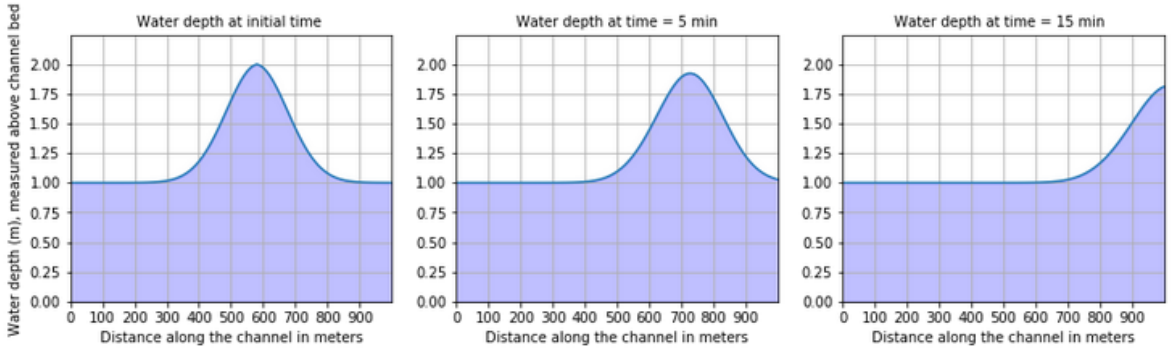

Figure 4.7: The Upwind method applied to a pulse in a ditch with a channel bed slope of 1 meter per kilometer ($S_0 = \frac{1}{1000}$), shown for the initial time and two later times. The final water depths in the ditch for $t \geq 30$ are 1 meter everywhere.

Thirdly, the Lax-Wendroff method was applied to the pulse in a ditch with a channel bed slope of 1 meter per kilometer. Figure 4.8 shows the pulse at the initial time and two later times. The Lax-Wendroff method produces results with a higher accuracy than the Upwind method. However, it also produces more oscillations in the result which can be seen in the roughness of the pulse at a time of 15 minutes. Similarly as above, it was not plotted that he final situation, for times $t \geq 30$, is a ditch with a water depth of 1 meter everywhere.

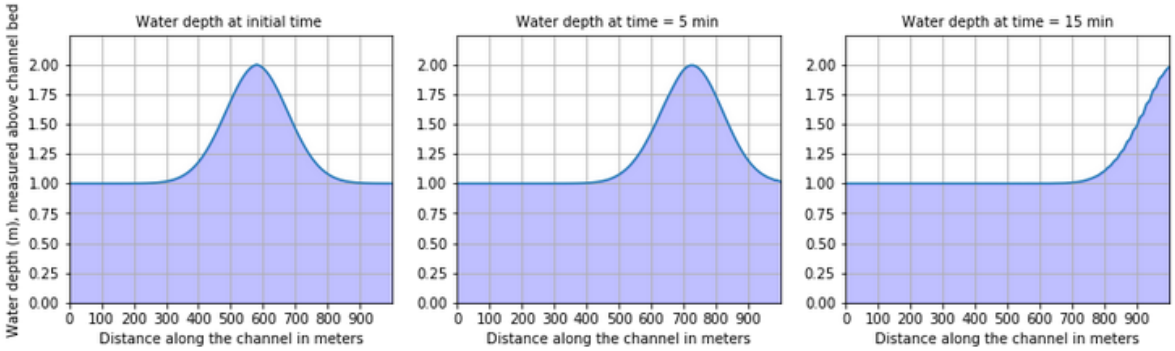

Figure 4.8: The Lax-Wendroff method applied to a pulse in a ditch with a channel bed slope of 1 meter per kilometer ($S_0 = \frac{1}{1000}$), shown for the initial time and two later times. The final water depths in the ditch for $t \geq 30$ are 1 meter everywhere.

External inflow Here, external inflow is considered. Imagine a big bucket of water being emptied in the middle of the ditch during the first minute. Let's see what happens to the water flow.

Firstly, the ditch with zero channel bed slope is considered again with $q(0,t) = 0 m^3/s$. Figure 4.9 illustrates this. It shows the water depth along the channel at the initial time, at half the time of emptying the bucket and at the time that the bucket is fully emptied. Similarly to the case of the pulse discussed above, the bucket of water does not move.

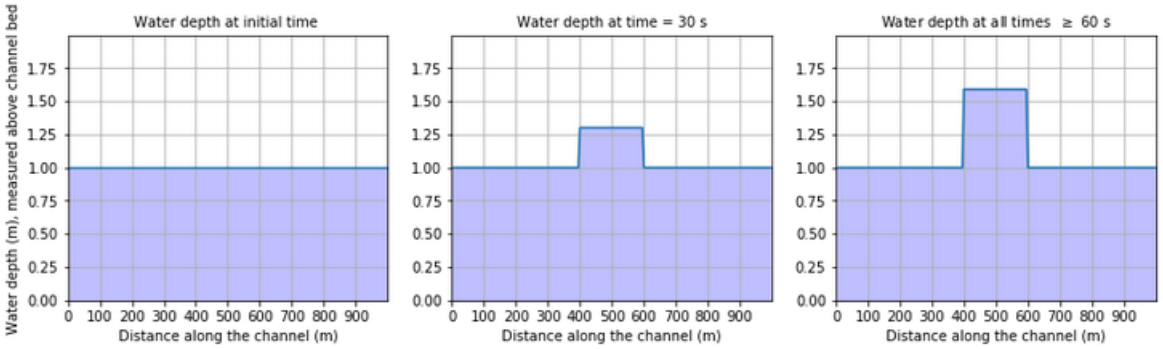

Figure 4.9: A bucket of water being emptied in a ditch with zero channel bed slope, so $S_0 = 0$. Hence, there is zero water flow at all times which results in a static bucket of water in a ditch.

Secondly, the Upwind method was applied to bucket of water case in a ditch with a channel bed slope of 1 meter per kilometer and $q(0,t) = 0.38\, m^3/s$. The bucket of water starts moving now. Figure 4.10 shows this movement starting at a time of 1 minute, which is the time at which the bucket has been fully emptied. The initial situation and the first minute were not plotted because they are similar to the case of a ditch with zero channel bed slope.

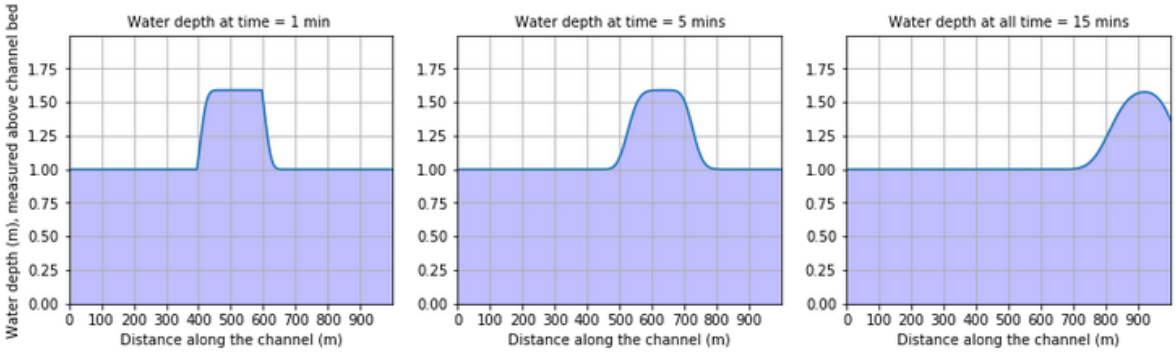

Figure 4.10: The Upwind method applied to a bucket of water being emptied in a ditch with a channel bed slope of 1 meter per kilometer ($S_0 = \frac{1}{1000}$), shown from a time onwards from which the bucket was fully emptied. The initial situation and the first minute is similar to the situations shown in Figure 4.9.

Thirdly, the Lax-Wendroff method was applied to a bucket of water being emptied in a ditch with a channel bed slope of 1 meter per kilometer and $q(0,t) = 0.38\, m^3/s$. Figure 4.11 shows the pulse at the initial time and two later times. Again, the Lax-Wendroff method produces more oscillations in the result which can be seen in the plots at all three times.

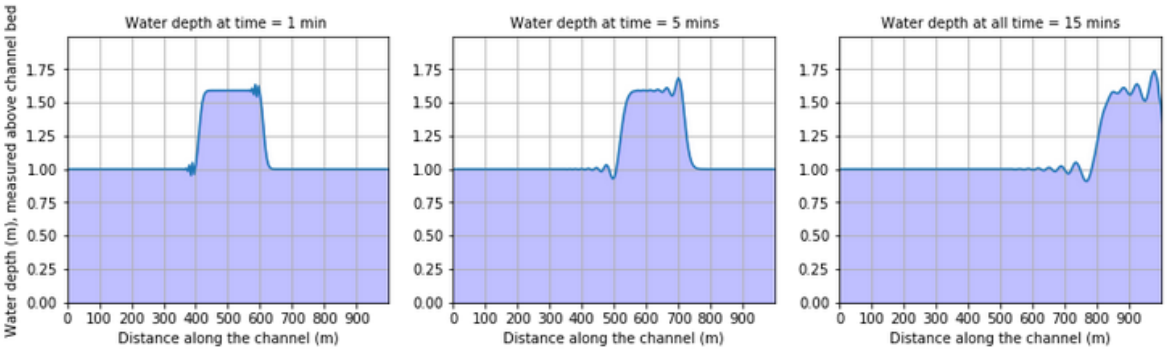

Figure 4.11: The Lax-Wendroff method applied to a bucket of water being emptied in a ditch with a channel bed slope of 1 meter per kilometer ($S_0 = \frac{1}{1000}$), shown from a time onwards from which the bucket was fully emptied. The initial situation and the first minute is similar to the situations shown in Figure 4.9.

4.5.3. Discussion

The results of the tests on the kinematic wave show that the kinematic wave successfully models the bulk movement of water flow in one direction when the ditch is sloped. However, ditches in a polder network are generally not designed with sloped channel beds so these slopes might be zero or very small. In addition, the water is only flowing in one direction and not spreading across the ditch. In the example of the external inflow of a bucket of water, this is against the intuition of the water spreading equally and flowing into two directions. Therefore, the kinematic wave equation does not seem to be the most realistic representation of water flow in a ditches network. However, it is a fast and simple method for computing the bulk of water flow when implemented with a small channel bed slope. One can think of applying the kinematic wave with an educated choice for a channel bed slope such that it models realistic water depths, velocities and discharges.

5

Testing the diffusion wave model

5.1. The diffusion wave model

The diffusion wave model is the next step towards a model that is closer to a realistic representation of the water flow. Although this thesis focuses on solving the kinematic wave, the option of extending the kinematic wave solution method to a diffusion wave solution method is investigated in this chapter. The diffusion wave model is formulated by

$$\begin{cases} \frac{\partial q}{\partial x} + \frac{\partial A}{\partial t} = I \\ \frac{\partial h}{\partial x} = S_0 - S_f \end{cases} \tag{5.1}$$

where q is discharge, h is the water depth above the channel bottom, A is the cross sectional area, I is the external in- or outflow, S_0 is the channel bed slope and S_f is the friction slope. The following paragraphs will discuss the interpretation and solution methods for the diffusion wave equation.

5.1.1. Interpretation and assumptions

First of all, hydrostatic pressure is assumed and the friction slope S_f is determined with Manning's equation as discussed in Section 3.2.1.

Kinematic waves do not attenuate as they move downstream, as was shown in the previous chapter. Diffusion waves also move downstream only, but attenuate as they move downstream. Accordingly, diffusion waves can model the so-called backwater effects. A backwater effect is the effect which a dam has in raising the water depths of the surface water upstream from it.

Similar to the kinematic wave model, for the diffusion wave model the water waves are also assumed to be long and traveling over relatively flat slopes. The *local acceleration* term $\frac{\partial q}{\partial t}$ and the *convective acceleration* term $\frac{\partial A}{\partial x}$ term are neglected in the equation of momentum. The pressure force term $S_p = \frac{\partial h}{\partial x}$ is included, which explains the attenuation of waves in the diffusion wave model.

5.1.2. The diffusion wave equation

The diffusion wave model (5.1) consists of the continuity equation

$$B\frac{\partial h}{\partial t}+\frac{\partial q}{\partial x}=I \tag{5.2}$$

together with a simplified form of the equation of motion; namely,

$$S_f = S_0 - S_p \tag{5.3}$$

With Manning's equation (3.1), assuming a perpendicular channel such that the cross sectional area is given by $A = Bh$ with fixed B, using the definition of discharge $q = Av$, $S_p = \frac{\partial h}{\partial x}$ and the definition of the hydraulic radius $R = A/P$ which in this case is $R = Bh/(2h+B)$, equation (5.3) can be expressed in the form

$$q = \frac{1}{n_m}\frac{(Bh)^{5/3}}{(2h+B)^{2/3}}\left(S_0-\frac{\partial h}{\partial x}\right)^{1/2} \tag{5.4}$$

By differentiating (5.4) with respect to x

$$\frac{\partial q}{\partial x} = \frac{1}{n_m}\frac{\partial}{\partial x}\frac{(Bh)^{5/3}}{(2h+B)^{2/3}}\left(S_0-\frac{\partial h}{\partial x}\right)^{1/2} \tag{5.5}$$

and plugging the resulting expression (5.5) into equation (5.2) one arrives at the diffusion wave equation in terms of the water depth h

$$\boxed{\frac{\partial h}{\partial t}+\frac{1}{n_m}\frac{\partial}{\partial x}\frac{(Bh)^{5/3}}{(2h+B)^{2/3}}\left(S_0-\frac{\partial h}{\partial x}\right)^{1/2}=\frac{1}{B}I} \tag{5.6}$$

5.2. Analytical solution of the diffusion wave model

The diffusion wave equation is a first-order nonlinear hyperbolic partial differential equation (PDE) to which the solution can be obtained in simple cases using the method of characteristics. The characteristic curves for the diffusion equation take the form

$$\begin{cases}\frac{\mathrm{d}h}{\mathrm{d}t} = I\\ c = \frac{1}{B}\frac{\mathrm{d}q}{\mathrm{d}h}\end{cases} \tag{5.7}$$

where the second equation in (5.7) for the wave celerity can be rewritten as follows

$$\frac{\mathrm{d}x}{\mathrm{d}t} = \frac{1}{B}\frac{\mathrm{d}q}{\mathrm{d}h} = \frac{1}{n_m}\frac{\mathrm{d}}{\mathrm{d}h}\frac{(Bh)^{5/3}}{(2h+B)^{2/3}}\left(S_0-\frac{\partial h}{\partial x}\right)^{1/2} \tag{5.8}$$

Solving these equations gives the solution which is constant along the characteristic curves.

5.3. Numerical solution of the diffusion wave model

Solving the diffusion wave equation resembles the process of solving the kinematic wave equation which was thoroughly discussed in Section 4.3. The only difference is the flux function. The solution method to the diffusion wave equation will be outlined in the following paragraph.

5.3.1. Numerical approximation of the diffusion wave equation

The diffusion wave equation (5.1) is a nonlinear conservation law of the form

$$h_t(x,t) + f(h(x,t))_x = \Psi(h(x,t),x,t) \tag{5.9}$$

where $f(h)$ is the flux function which governs the fluxes in and out of the finite volumes and $\Psi(h(x,t),x,t)$ is the source function which accounts for external effects that change the quantity of interest in addition to the fluxes. In the case of the diffusion wave, the flux function is $f(h(x,t)) = \frac{1}{n_m}\frac{(Bh)^{5/3}}{(2h+B)^{2/3}}\left(S_0 - \frac{\partial h}{\partial x}\right)^{1/2}$ and the source function $\Psi(h(x,t),x,t) = I(h(x,t),x,t)$ accounts for external in- or outflows.

The numerical approximation of the solution to the diffusion wave equation works in a similar way as the approximation of the kinematic wave equation described in Section 4.3.3, with the flux function being the only difference. Hence, formulated as in the fractional step method, the problem reads

$$\text{Problem A: } h_t + \left(\frac{1}{n_m}\frac{(Bh)^{5/3}}{(2h+B)^{2/3}}\left(S_0 - \frac{\partial h}{\partial x}\right)^{1/2}\right)_x = 0 \tag{5.10}$$

$$\text{Problem B: } h_t = I(h(x,t),x,t) \tag{5.11}$$

to which the solution method is formulated as

$$H_i^{n+1} = H_i^n - \frac{\Delta t}{\Delta x}[(s_{i+1/2})^-(H_{i+1}^n - H_i^n) - (s_{i-1/2})^+(H_i^n - H_{i-1}^n)] + \Delta t\frac{1}{B}I \tag{5.12}$$

The flux function is trickier for the diffusion wave since firstly, it contains the derivative $\frac{\partial h}{\partial x}$ and secondly, it contains a square root of $S_0 - S_p$ which only gives reasonable results if $S_0 \geq S_p$. When $S_0 \leq S_p$, Equation (5.6) becomes parabolic instead of hyperbolic. Therefore, the developed methods for solving the kinematic wave equation cannot simply be extended to the diffusion wave equation. This extension only works provided that $S_0 \geq S_p$.

In the following sections, results of the application of Equation (5.12) to the diffusion wave are given for examples in which $S_0 \geq S_p$ holds in the entire domain for every time step. Herein, the wavespeeds $s_{i-1/2}$ are defined as, similarly to Equation (4.22),

$$s_{i-1/2} = \begin{cases} [f(H_{i-1},H_i) - f(H_{i-2},H_{i-1})]/(H_i - H_{i-1}) \\ f'(H_{i-1},H_i) \end{cases} \tag{5.13}$$

Here, the flux function depends on two grid cells because of the pressure term $S_p = \frac{\partial h}{\partial x}$ in the flux function. The numerically discretized flux function is given by

$$f(H_{i-1},H_i) = \frac{1}{n_m}\frac{(BH_i)^{5/3}}{(2H_i+B)^{2/3}}\left(S_0 - \frac{H_i - H_{i-1}}{\Delta x}\right)^{1/2} \tag{5.14}$$

and its derivative is given by

$$f'(H_{i-1},H_i) = \frac{B^{5/3}}{n_m}\frac{5(S_0 - (H_i - H_{i-1})/\Delta x)^{1/2}H_i^{2/3}}{3(2H_i+B)^{2/3}} - \frac{B^{5/3}}{n_m}\frac{4(S_0 - (H_i - H_{i-1})/\Delta x)^{1/2}H_i^{5/3}}{3(2H_i+B)^{5/3}} \tag{5.15}$$

5.4. Verification of the developed numerical methods

The method of manufactured solutions is applied to the method developed in the previous Section 5.3.1. Similarly to what was done for the kinematic wave, the solution $h(x,t) = \frac{3}{2} - \sin(t-x)$ is assumed and plugged

into the diffusion equation (5.6). It gives a boundary condition of $h(0,t) = \frac{3}{2} - \sin(t)$, an initial condition of $h(x,0) = \frac{3}{2} + \sin(x)$ and a source function of

$$\frac{1}{B} I = \frac{B^{5/3}}{n_m} [\frac{5(S_0 - \cos(t-x))^{1/2} \cos(t-x)(3/2 - \sin(t-x))^{2/3}}{3(B + 2(3/2 - \sin(t-x)))^{2/3}} \tag{5.16}$$

$$- \frac{4(S_0 - \cos(t-x))^{1/2} \cos(t-x)(3/2 - \sin(t-x))^{5/3}}{3(B + 2(3/2 - \sin(t-x)))^{5/3}} \tag{5.17}$$

$$- \frac{(3/2 - \sin t - x))^{5/3} \sin(t-x)}{2(S_0 - \cos(t-x))^{1/2} (B + 2(3/2 - \sin(t-x)))^{2/3}}] \tag{5.18}$$

Implementing these conditions with the developed numerical method should result in the assumed solution $h(x,t) = \frac{3}{2} - \sin(t-x)$. The results are given in Figure 5.1

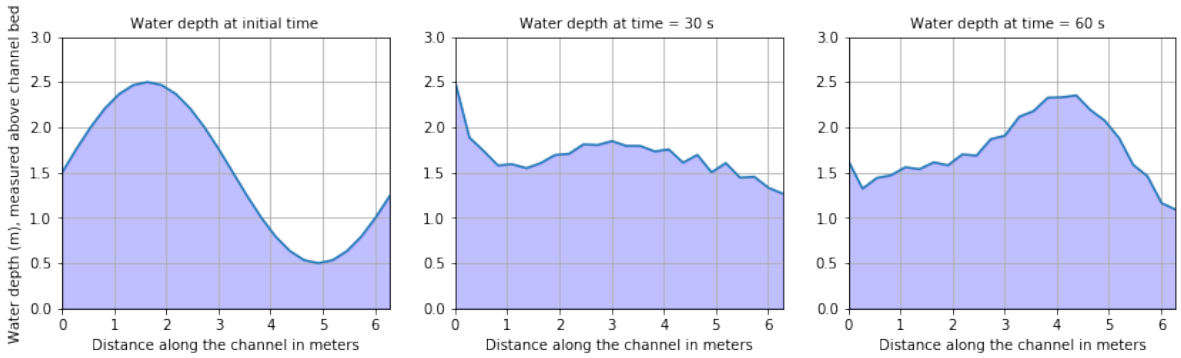

Figure 5.1: The results for the method of manufactured solutions to the diffusion wave Upwind numerical method. Clearly, the results do not match the assumed solution. Therefore, the numerical methods were not developed successfully yet and adjustments need to be made.

Clearly, the assumed solutions breaks immediately in the first minute. Therefore, the developed methods are not working properly. This can be due to incorrect implementation of the Dirichlet boundary conditions or unjust discretization of the derivative term $S_p = \frac{\partial h}{\partial x}$ in the flux term. How to improve the results of this numerical method is a point for further research.

5.5. Application to a straight ditch

The developed method for the diffusion wave model was not successfully verified. Therefore, the results from the model are not easily comparable to the kinematic wave results. However, the developed solution method for the diffusion wave works in a few cases. These cases were implemented to give the reader an idea of the possibilities with the diffusion wave model.

To illustrate the impossible comparison between the tests of the kinematic wave with the diffusion wave, the case of channel bed slope $S_0 = \frac{1}{1000}$ and Gauckler-Manning coefficient of $n_m = 0.04$ is implemented for a ditch of width 1 meter and length 1000 meter. Figure 5.2 shows the results. Clearly, the wave does not seem to move as smoothly as the kinematic wave applied to the same case shown in Figure 4.7. The wave shows breaking results due to negative values in the square root $\sqrt{S_0 - \frac{\partial h}{\partial x}}$ in the flux function.

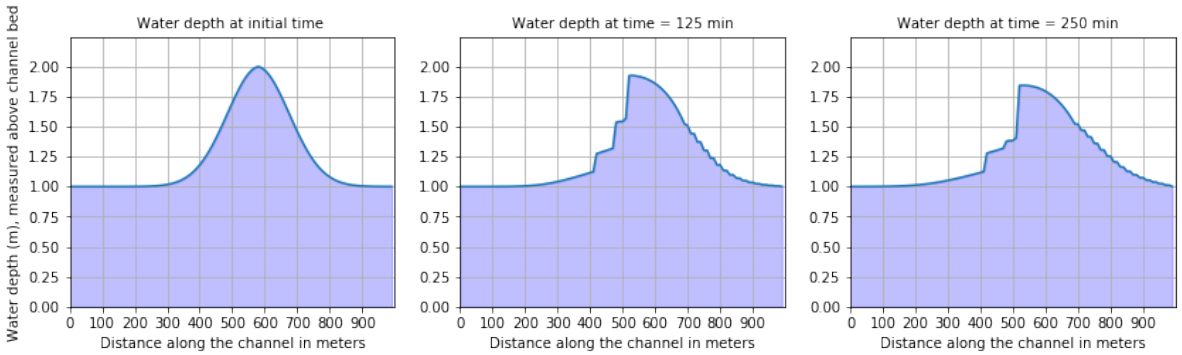

Figure 5.2: The results of the Upwind method for the diffusion wave with channel bed slope $S_0 = \frac{1}{1000}$ and Gauckler-Manning coefficient $n_m = 0.04$.

Now, to give the reader an idea of what results the diffusion wave model should give, the method was implemented for very large channel bed slopes of $S_0 = 1$. This causes the square root in the flux function to attain positive values only. Figure 5.3 shows the results for the Upwind method, Figure 5.4 shows the results of the Lax-Wendroff method. These results are very similar to the results for the kinematic waves. The main difference is that the diffusion waves travel much slower.

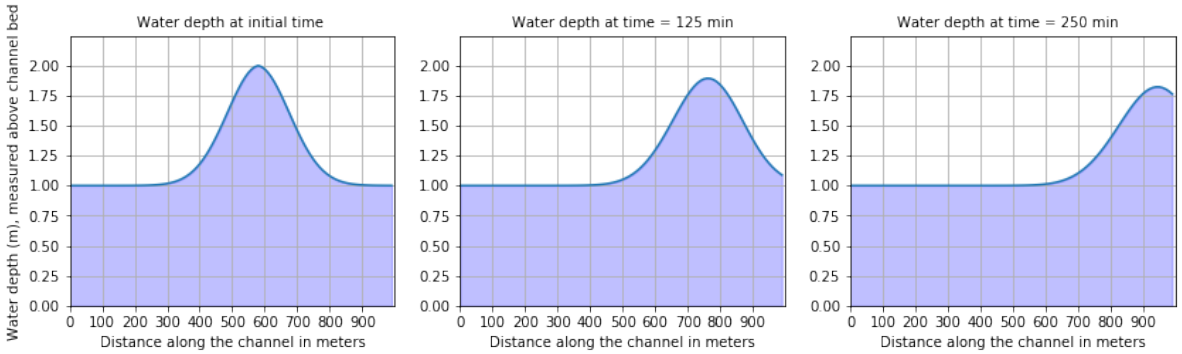

Figure 5.3: The Upwind method for the diffusion wave with large channel bed slope $S_0 = 1$ and Gauckler-Manning $n_m = 0.04$.

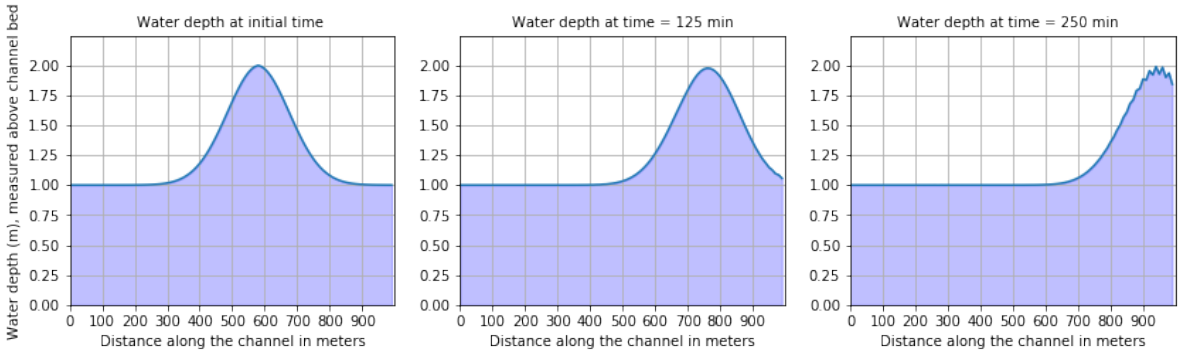

Figure 5.4: The Lax-Wendroff method for the diffusion wave with large channel bed slope $S_0 = 1$ and Gauckler-Manning $n_m = 0.04$.

Interestingly, in the case of a pulse with zero initial depths around it, the backwater effects are better visible. See Figure 5.5.

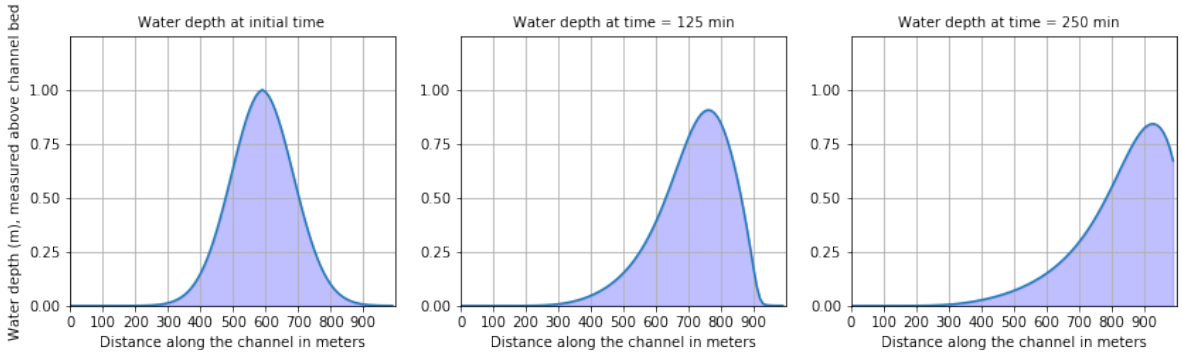

Figure 5.5: The Upwind method for the diffusion wave with large channel bed slope $S_0 = 1$ and Gauckler-Manning $n_m = 0.04$.

5.5.1. Discussion

The diffusion wave model was only successfully implemented for a few cases with high channel bed slopes. The behavior of the wave flows seem very similar to the behavior shown by the kinematic wave movement. Breaking of the solutions as was visible in Figure 5.1 shows that the numerical methods developed for the kinematic wave equation cannot simply be applied to the diffusion wave equation as well. The issue may be with the discretization of the derivative $\frac{\partial h}{\partial x}$. It might also be a stability issue. The flux function (5.14) takes complex values for small channel bed slopes, hence the equation becomes non-hyperbolic according to Leveques hyperbolicity properties given on page 1-3 of [12] . Therefore, the developed explicit methods work well for the hyperbolic kinematic wave equation. Different explicit or even implicit numerical solution methods may be necessary to take care of stability issues when solving the diffusion wave equation. More research needs to be done into suitable numerical solution methods such that the diffusion wave equation works well for small channel bed slopes and such that the backwater effects are incorporated sufficiently. A variety of different approaches on how to implement the diffusion wave model are discussed in for example [16–19].

6

Testing the dynamic wave model

6.1. The dynamic wave model

In this chapter, a finite volume method for a system of two equations is developed to model water flow using the full shallow water equations

$$\begin{cases} \frac{\partial A}{\partial t} + \frac{\partial q}{\partial x} = I \\ \frac{\partial q}{\partial t} + \frac{\partial qv}{\partial x} = gA(S_0 - S_f - S_p) \end{cases} \tag{6.1}$$

This model is often referred to as the dynamic wave model. It produces the most theoretically accurate results because it models the full shallow water equations. Whereas the kinematic wave models water flow driven by gravity into one flow direction, the dynamic wave model is driven by local and convective acceleration plus friction, pressure and gravity forces. Therefore, dynamic waves attenuate as they travel in both upstream and downstream directions as is illustrated in Figure 6.1. Accordingly, the dynamic wave model accounts for backwater effects, flow reversal and zero-slope water flow [20].

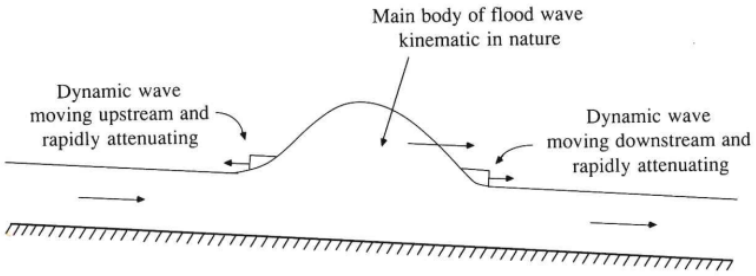

Figure 6.1: The nature of dynamic waves as is illustrated in Figure 9.3.2 in Chow [8]

6.2. Solution of the shallow water equations

The full shallow water equations form a system of two nonlinear hyperbolic equations. Analytical solutions to this system can be found for simple cases with the method of characteristics. When external inflows are

negligible, the characteristic equations are given by

$$\begin{cases} \frac{dx}{dt} = v \pm c_d \\ \frac{d}{dt}(v \pm 2c_d) = g(S_0 - S_f) \end{cases} \tag{6.2}$$

in which $c_d = \sqrt{gh}$ is the dynamic wave celerity for a rectangular channel [8].

Instead of solving these characteristic equations analytically, the focus of this research is on the numerical approximation of the solution of the shallow water equations. Hence, the following sections outline the build up to the numerical method. First, the case of a system of two linear equations is discussed followed by the method for the full shallow water equations.

6.2.1. Numerical approximation of a system of two linear equations

Before going on to the numerical approximation of the shallow water equations, a system of two equations for a multicomponent advection equation will be discussed. Subsequently, the developed solution methods can be applied to the more complex case of the shallow water equations.

Here, the methods are similar to those discussed in Section 4.3.2. The advection equation takes the form

$$w_t(x,t) + Aw_x(x,t) = 0 \tag{6.3}$$

with the vector $w \in \mathbb{R}^2$ and matrix $A \in \mathbb{R}^{2\times 2}$. The finite volume method, as also given in Equation (4.16), is

$$W_i^{n+1} = W_i^n - \frac{\Delta t}{\Delta x}\left[\mathcal{F}(W_i^n, W_{i+1}^n) - \mathcal{F}(W_{i-1}^n, W_i^n)\right] \tag{6.4}$$

in which $F_{i-1/2}^n = \mathcal{F}(W_{i-1}, W_i)$ is the average flux at point $x_{i-1/2}$ defined by the flux function $\mathcal{F}$. These flux functions can take different forms, depending on the finite volume method. The Upwind and Lax-Wendroff methods will be considered.

Upwind flux In the scalar case in Section 4.3.2, there is one wave traveling into cell C_i; either a wave $\mathcal{W}_{i-1/2}$ with positive velocity λ^+ or a wave $\mathcal{W}_{i+1/2}$ with negative velocity λ^-. Now, in the case of a linear system of two equations, there are two waves ($\mathcal{W}_1$ and $\mathcal{W}_2$) traveling into cell C_i with distinct wave velocities corresponding to the eigenvalues of matrix A. The waves are defined slightly differently in case of the constant-coefficient linear system; namely,

$$\mathcal{W}_{p,i-1/2} = \alpha_{p,i-1/2} r_p \tag{6.5}$$

for $p \in \{1,2\}$ where r_p is the p-th eigenvector of A. $\alpha_{p,i-1/2}$, $p \in \{1,2\}$, is defined as follows.The wave $\mathcal{W} = W_i - W_{i-1}$ in a cell C_i is decomposed into the eigenvectors of A

$$W_i - W_{i-1} = \alpha_{1,i-1/2} r_1 + \alpha_{2,i-1/2} r_2$$

Hence, the vector is $\alpha_{i-1/2} = R^{-1}(W_i - W_{i-1}) \in \mathbb{R}^2$, where $R = [r_1 \quad r_2]$ is the matrix composed of the eigenvectors of A. Hence, adding up the effects of the two waves $\mathcal{W}_1$ and $\mathcal{W}_2$ results in the flux functions

$$F_{i+1/2}^n = \lambda_1^- \mathcal{W}_{1,i+1/2} + \lambda_2^- \mathcal{W}_{2,i+1/2} = \lambda_1^- \alpha_{1,i+1/2} r_1 + \lambda_2^- \alpha_{2,i+1/2} r_2$$
$$F_{i-1/2}^n = \lambda_1^+ \mathcal{W}_{1,i-1/2} + \lambda_2^+ \mathcal{W}_{2,i-1/2} = \lambda_1^+ \alpha_{1,i-1/2} r_1 + \lambda_2^+ \alpha_{2,i-1/2} r_2$$

where λ_1 is the wave speed corresponding to wave $\mathcal{W}_1$ and λ_2 is the wave speed corresponding to wave $\mathcal{W}_2$. λ_p^+ and λ_p^- for $p \in \{1,2\}$ are defined according to Equation (4.17). Again, note that either λ_p^+ or λ_p^-, $p \in \{1,2\}$, is zero according to this definition. The upwind finite volume method (6.4) becomes

$$W_i^{n+1} = W_i^n - \frac{\Delta t}{\Delta x}\left[(\lambda_1^- \alpha_{1,i+1/2} r_1 + \lambda_2^- \alpha_{2,i+1/2} r_2) - (\lambda_1^+ \alpha_{1,i-1/2} r_1 + \lambda_2^+ \alpha_{2,i-1/2} r_2)\right] \tag{6.6}$$

To verify above equation, it was implemented for the case of Equation (6.3) with the matrix

$$A = \begin{pmatrix} -1 & 0 \\ 0 & 2 \end{pmatrix}$$

which gives $\lambda_1 = -1$, $\lambda_2 = 2$, $r_1 = [1 \quad 0]^T$ and $r_2 = [0 \quad 1]^T$. Thus, Equation (6.4) takes the form

$$W_i^{n+1} = W_i^n - \frac{\Delta t}{\Delta x}\left[\lambda_1 \alpha_{1,i+1/2} r_1 - \lambda_2 \alpha_{2,i-1/2} r_2\right]$$

in which $\lambda_1^- = \lambda_1$ and $\lambda_2^+ = \lambda_2$. Periodic boundary conditions were used for this test implementation. Figure 6.2 shows the solution for this system of equations with a CFL condition of $dt = 0.4dx$ at time $t = 1$.

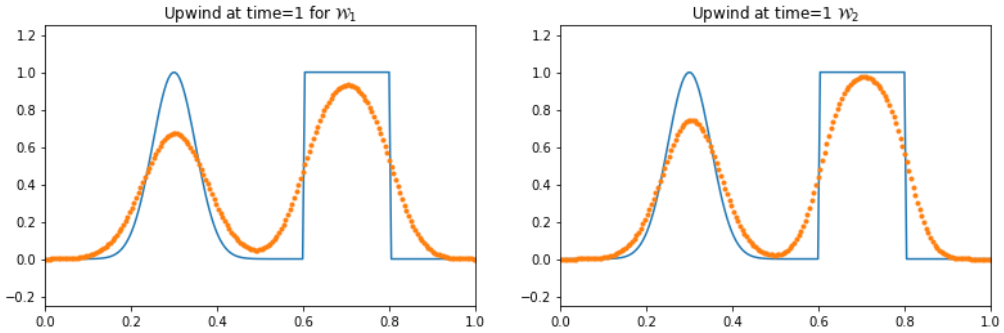

Figure 6.2: Solution of the upwind method for the system of the multicomponent advection equation for a CFL condition of $dt = .4dx$

Lax-Wendroff flux The Lax-Wendroff method incorporates flux correction terms $\tilde{F}$. It is given by

$$W_i^{n+1} = W_i^n - \frac{\Delta t}{\Delta x}\left[(\lambda_1^- \alpha_{1,i+1/2} r_1 + \lambda_2^- \alpha_{2,i+1/2} r_2) - (\lambda_1^+ \alpha_{1,i-1/2} r_1 + \lambda_2^+ \alpha_{2,i-1/2} r_2)\right] \tag{6.7}$$

$$- \frac{\Delta t}{\Delta x}(\tilde{F}_{i+1/2} - \tilde{F}_{i-1/2}) \tag{6.8}$$

In the Lax-Wendroff method for linear systems, $\tilde{F}_{i-1/2}$ is defined as

$$\tilde{F}_{i-1/2} = \frac{1}{2}\left(|\lambda_1|(1 - \frac{\Delta t}{\Delta x}|\lambda_1|)\alpha_{1,i-1/2} r_1 + |\lambda_2|(1 - \frac{\Delta t}{\Delta x}|\lambda_2|)\alpha_{2,i-1/2} r_2\right) \tag{6.9}$$

Implementing above equation to the same system as applied for the Upwind method, gives the solutions shown in Figure 6.3 for time $t = 1$.

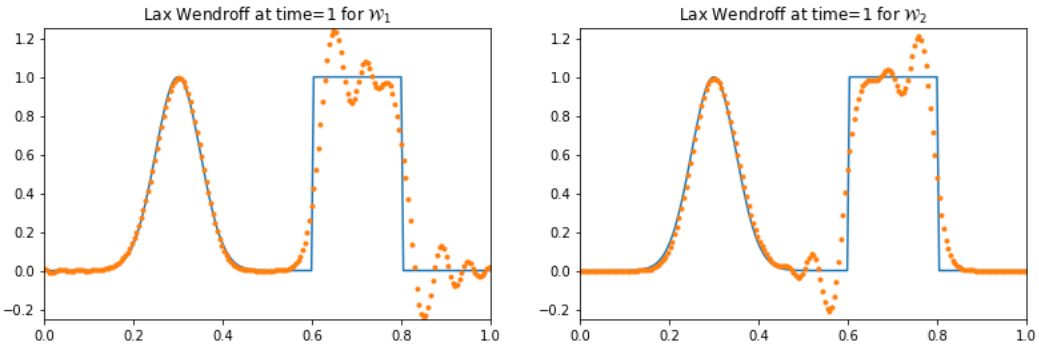

Figure 6.3: Solution of the Lax-Wendroff method for the multicomponent advection equation for a CFL condition of $dt = .4dx$

6.2.2. Numerical approximation of the shallow water equations

Equation (6.1) can be rewritten, using that $A = Bh$, $q = vA$ and $S_p = \frac{\partial h}{\partial x}$, as

$$\begin{cases} \frac{\partial h}{\partial t} + \frac{\partial hv}{\partial x} = \frac{1}{B} I \\ \frac{\partial (hv)}{\partial t} + \frac{\partial (hv)^2}{\partial x} + gh\frac{\partial h}{\partial x} = gh(S_0 - S_f) \end{cases} \tag{6.10}$$

For simplicity, let us first consider the case where $I = 0$ and $S_0 - S_f = 0$ so that the source terms in (6.10) vanish yielding the system of equations

$$\begin{cases} \frac{\partial h}{\partial t} + \frac{\partial hv}{\partial x} = 0 \\ \frac{\partial (hv)}{\partial t} + \frac{\partial}{\partial x}(hv^2 + \frac{1}{2}gh^2) = 0 \end{cases} \tag{6.11}$$

The system of equations becomes

$$\begin{bmatrix} h \\ hv \end{bmatrix}_t + \begin{bmatrix} hv \\ \frac{1}{2}v^2 + gh \end{bmatrix}_x = 0 \tag{6.12}$$

Let's define $w(x,t) = \begin{bmatrix} h \\ hv \end{bmatrix} = \begin{bmatrix} w_1 \\ w_2 \end{bmatrix}$, $f(w) = \begin{bmatrix} hv \\ \frac{1}{2}v^2 + gh \end{bmatrix} = \begin{bmatrix} w_2 \\ (w_2)^2/w_1 + \frac{1}{2}(w_1)^2 \end{bmatrix}$. Hence, for smooth solutions this system of equations can be formulated in the quasilinear form

$$w_t + f'(w)w_x = 0$$

with the Jacobian matrix $f'(w)$

$$f'(w) = \begin{bmatrix} 0 & 1 \\ -(w_2/w_1)^2 + gw_1 & 2w_2/w_1 \end{bmatrix} = \begin{bmatrix} 0 & 1 \\ -v^2 + gh & 2v \end{bmatrix} \tag{6.13}$$

which results in the eigenvalues

$$\lambda_1 = v - \sqrt{gh}, \qquad \lambda_2 = v + \sqrt{gh} \tag{6.14}$$

and eigenvectors

$$r_1 = \begin{bmatrix} 1 \\ v - \sqrt{gh} \end{bmatrix}, \qquad r_2 = \begin{bmatrix} 1 \\ v + \sqrt{gh} \end{bmatrix} \tag{6.15}$$

which can be implemented with the Upwind or Lax-Wendroff finite volume methods (6.6) and (6.7) discussed in the previous paragraphs. Hence, this is the linearized system of the shallow water equations.

Now, the fractional step method is used to add the source term $\Psi(h(x,t),v(x,t),x,t) = \begin{bmatrix} \frac{1}{B}I \\ gh(S_0 - S_f) \end{bmatrix}$ to the system of equations. Finding the solution of the shallow water equations is separated into two problems:

$$\text{Problem A: } \begin{bmatrix} h \\ hv \end{bmatrix}_t + \begin{bmatrix} hv \\ \frac{1}{2}v^2 + gh \end{bmatrix}_x = 0 \tag{6.16}$$

$$\text{Problem B: } \begin{bmatrix} h \\ hv \end{bmatrix}_t = \begin{bmatrix} \frac{1}{B}I \\ gh(S_0 - S_f) \end{bmatrix} \tag{6.17}$$

The method is similar to what was done for adding the source term in the kinematic wave equation. In the first step, the upwind method, or any other method, is applied. In the second step, the forward Euler for the ODE of problem B is applied. Accordingly, considering the Upwind method,

$$\text{A-step: } H_i^* = H_i^n - \frac{\Delta t}{\Delta x}\left[(\lambda_1^- \alpha_{1,i+1/2} r_1 + \lambda_2^- \alpha_{2,i+1/2} r_2) - (\lambda_1^+ \alpha_{1,i-1/2} r_1 + \lambda_2^+ \alpha_{2,i-1/2} r_2)\right] \tag{6.18}$$

$$\text{B-step: } H_i^{n+1} = H_i^* + \Delta t \begin{bmatrix} \frac{1}{B}I \\ gh(S_0 - S_f) \end{bmatrix} \tag{6.19}$$

which is rewritten by eliminating H_i^* as follows

$$H_i^{n+1} = H_i^n - \frac{\Delta t}{\Delta x}\left[(\lambda_1^- \alpha_{1,i+1/2} r_1 + \lambda_2^- \alpha_{2,i+1/2} r_2) - (\lambda_1^+ \alpha_{1,i-1/2} r_1 + \lambda_2^+ \alpha_{2,i-1/2} r_2)\right] + \Delta t \begin{bmatrix} \frac{1}{B}I \\ gh(S_0 - S_f) \end{bmatrix} \tag{6.20}$$

6.3. Necessary and sufficient conditions

Proving theoretical convergence for the methods of approximating nonlinear systems of equations is not proven yet, and beyond the scope of this thesis. However, the methods used here are generally successful in practice [12]. Importantly, the CFL condition should hold for both equations of the shallow water equations. The condition

$$\frac{\Delta t}{\Delta x}\max|f'(h)| \leq \frac{1}{2} \tag{6.21}$$

is to be satisfied for every value of $h = H_i$ in the computations.

6.4. Verification of the developed numerical methods

Verifying the Upwind method and the Lax-Wendroff method for the shallow water equations is done by using the results given in Leveque, on page 257 [12]. The evolution of a hump of water is considered in a zero channel bed sloped ditch, with zero initial velocity in which the source term of the shallow water equations is set to zero as well $\Psi(h(x,t),v(x,t),x,t) = 0$.

Figure 6.4: The results of the developed method for the shallow water equations for a hump of water with zero initial velocity and with zero source terms. The same initial data was considered as in [12] and the results turn out similar to those given on page 257 [12]. The figure on the left show the water depths and the figures on the right show the depths times the water velocities, which equals the discharges when the width is $B = 1$.

Important to mention is that the verification above was done for the case without external inflows. Therefore, the method is still to be verified for the case of non-zero external inflows. The results when implementing the fractional step methods seemed reasonable. Therefore, the case of emptying a water bucket in a ditch is implemented and included in the next section. Verification of the numerical method with nonzero inflows is a point for further research.

6.5. Implementation

6.5.1. Initial solution and boundary conditions

Initial solution Just as before, an initial solution needs to be specified and two different initial solutions will be considered; namely, a pulse without external inflow and a flat water level with external inflow. The cases of a zero channel bed slope and a small channel bed slope will be compared again.

Boundary conditions In the case of the full shallow water equations, both the inflow and the outflow boundary need to have assigned values. Generally, a discharge for the upstream boundary is set and a water depth for the downstream boundary is set. Accordingly, the upstream water depth and the downstream discharge are calculated from these values.

Inflow boundary

The inflow boundary in the following test cases was set to a value of $vh = 0$. Hence, there is no water inflow. To enable the numerical computation, a ghost cell was assigned on the left of the first grid cell. The ghost cell's value was set by zero order extrapolation

$$H_{-1}^n = H_0^n$$

.

Outflow boundary

The outflow boundary in the following test cases was set to a water depth of 1 meter. Similarly to the inflow boundary, a ghost cell was placed on the right of the outflow boundary cell. Its value was also set by zero order extrapolation

$$H_N^n = H_{N+1}^n$$

6.5.2. Results

No external inflow The flow behavior of a water pulse was investigated for the case of zero external inflows. In all these test cases the ditch is set to be of length 1 km, width 1 m, with a Gauckler-Manning coefficient of $n_m = 0.04$. The Dirichlet upstream boundary condition is set to a value of $vh = 0$ and the downstream boundary condition is set to a water depth of 1 meter. A zero channel bed slope is assumed since since ditches in a Dutch polder network generally have zero channel bed slopes.

Firstly, in Figure 6.5 the Upwind method for the shallow water equations is considered. The initial solution is the same pulse as was applied in Section 4.5.2. The boundary conditions were implemented as outlined in Section 6.5.1. The Upwind method produces a smooth solution. It shows that the pulse dissipates in both directions and stabilizes around 60 minutes time.

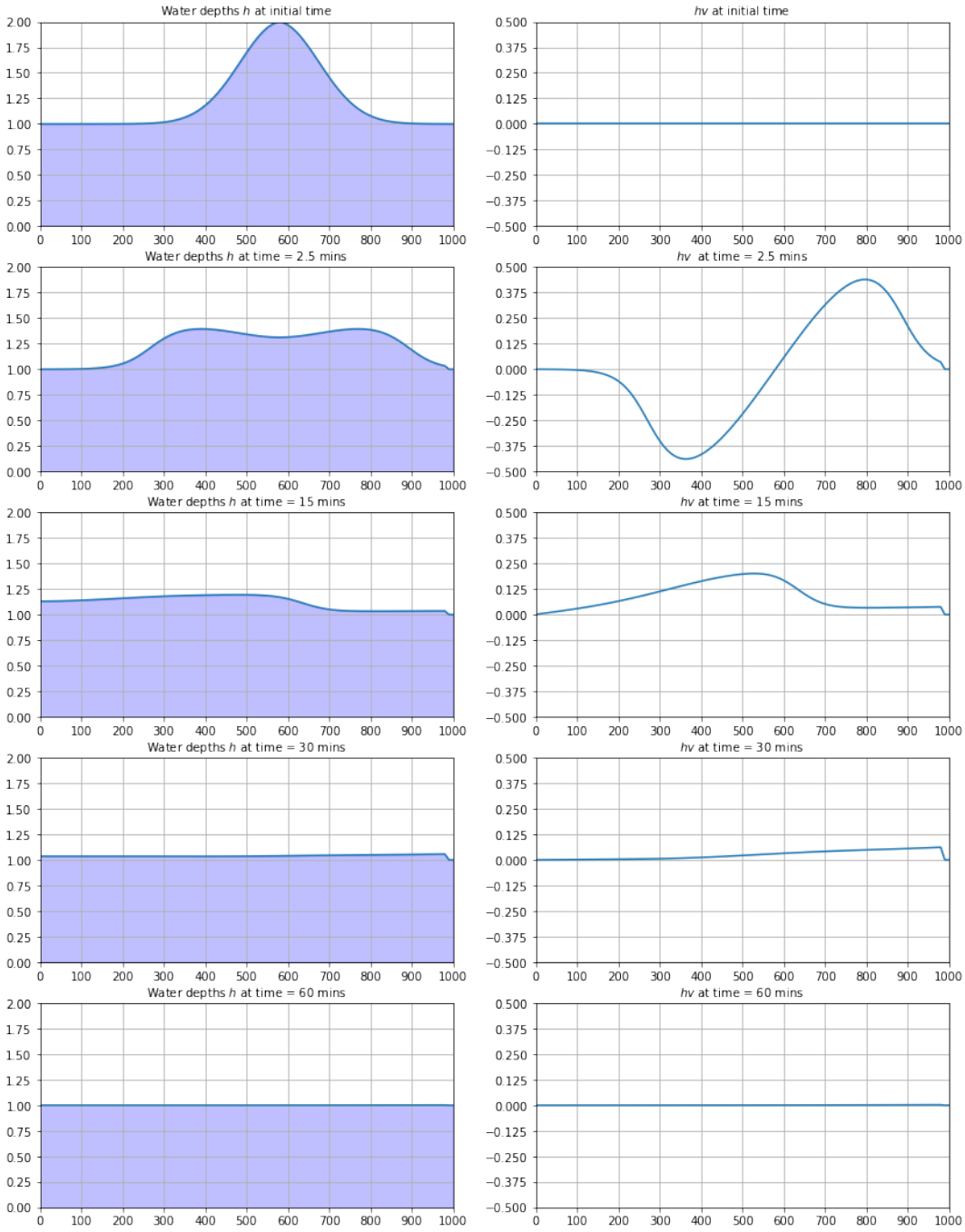

Figure 6.5: The Upwind method of the shallow water equations applied to a pulse in a zero channel bed sloped ditch. The data for the initial pulse is the same as was used for the kinematic and diffusive wave test results.

Secondly, in Figure 6.6 the Lax-Wendroff method for the shallow water equations is considered applied to the pulse with the same boundary conditions mentioned above. The Lax-Wendroff method shows results with an accuracy of $\mathcal{O}(\Delta x^2)$ but with oscillatory behavior. A so-called flux-limiter method could be applied to the finite volume method to smoothen its oscillatory behavior [12]. However, this is a point for further research.

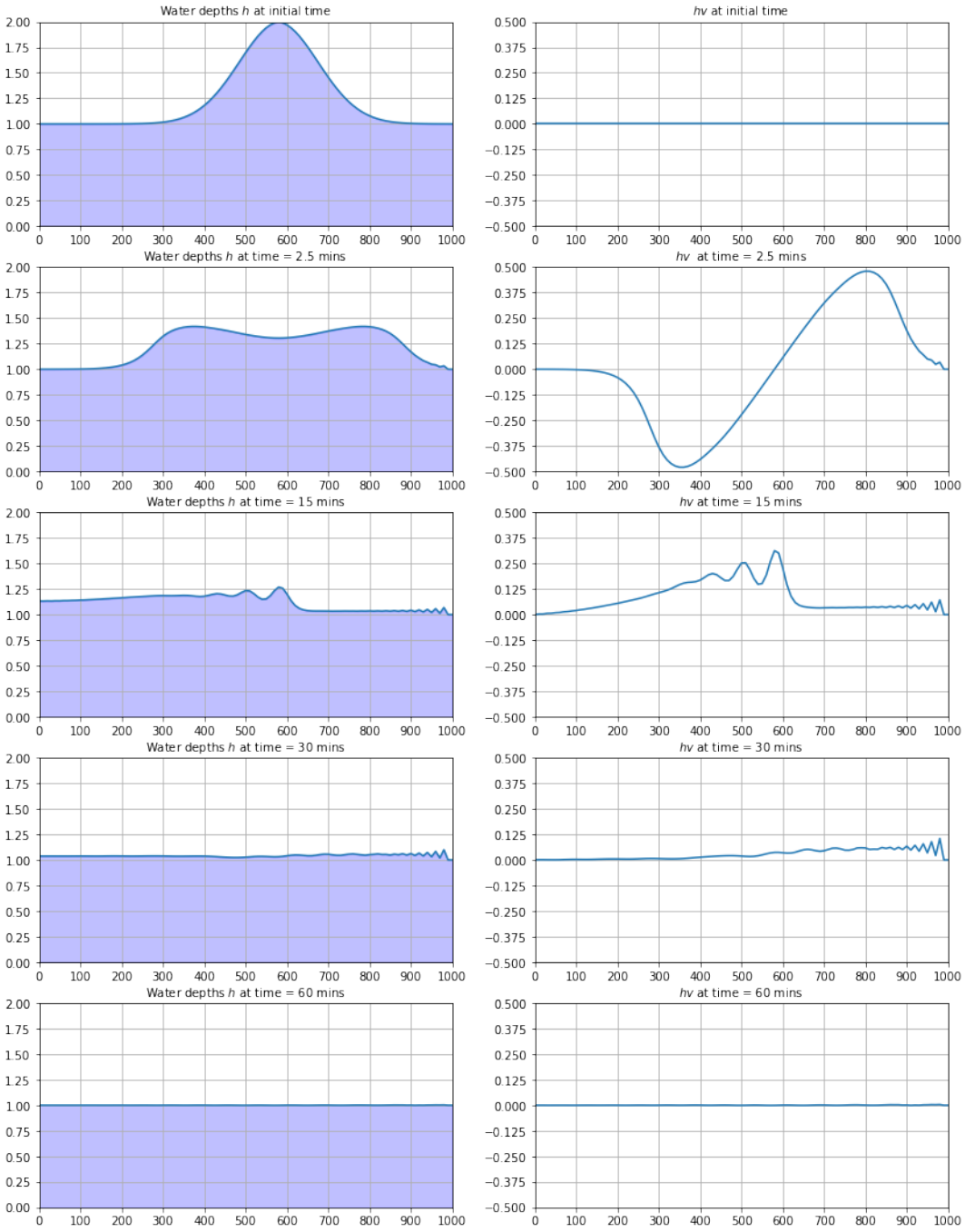

Figure 6.6: The Lax-Wendroff method of the shallow water equations applied to a pulse in a zero channel bed sloped ditch. The data for the initial pulse is the same as was used for the kinematic and diffusive wave test results.

External inflow Here, external inflow is considered. Again, a big bucket of water is emptied in the middle of the ditch during the first minute. Firstly, the Upwind method for the shallow water equations applied to a ditch with zero channel bed slope is considered again. Figure 6.7 illustrates this.

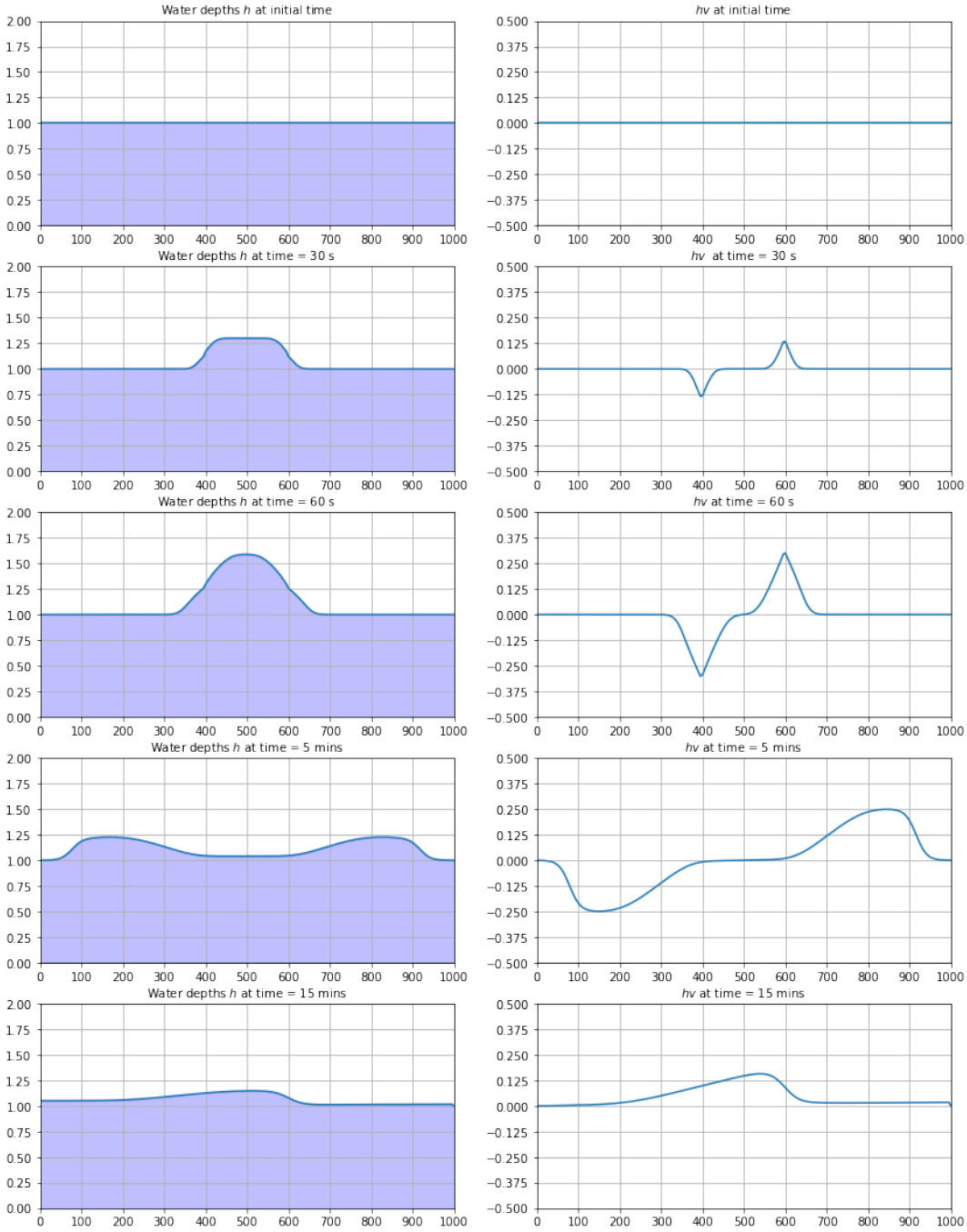

Figure 6.7: The Upwind method of the shallow water equations applied to a bucket of water being emptied in a zero channel bed sloped ditch.

Secondly, the Lax-Wendroff method for the shallow water equations applied to a ditch with zero channel bed slope is considered. Figure 6.8 illustrates this.

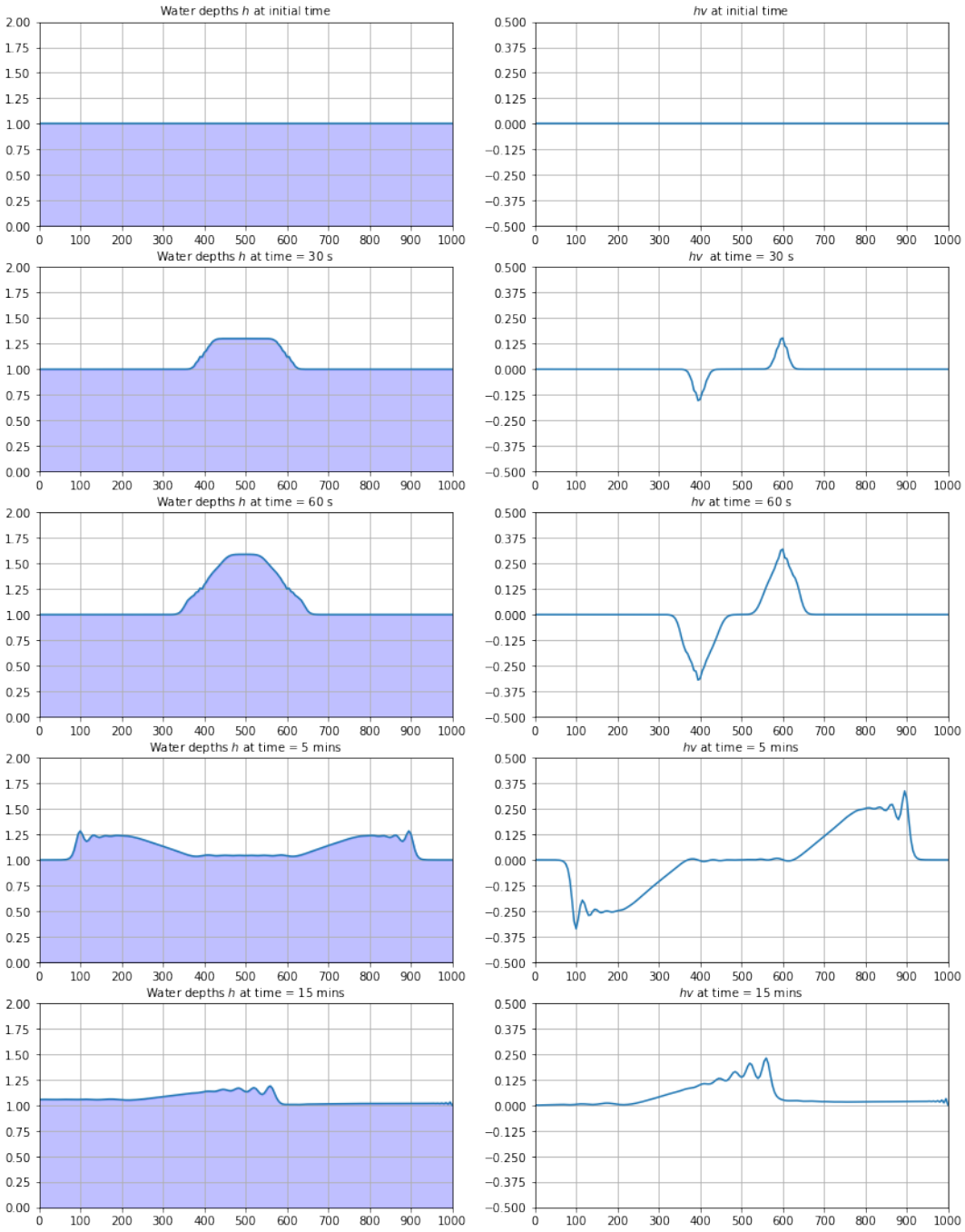

Figure 6.8: The Lax-Wendroff method of the shallow water equations applied to a bucket of water being emptied in a zero channel bed sloped ditch.

6.5.3. Discussion

Upwind and Lax-Wendroff finite volume methods were developed for solving the system of the full shallow water equations. This is a more complicated, computationally demanding solution method in comparison to the methods for the kinematic and the diffusion waves because of the nonlinearity of both shallow water equations. However, the full shallow water equations model waves that propagate and dissipate into both directions of a ditch. Therefore, the type of water flow that is modeled is as close as one can get to reality for a ditches network in a Dutch polder.

7

Comparison of the various methods

7.1. General

Three different approaches to modeling water flow were discussed in Chapters 4, 5 and 6; namely, the kinematic wave equation, the diffusion wave equation and the dynamic wave equations. In this section, the performance of each of the approaches and their potential applicability to a Dutch polder network will be discussed.

7.2. Computational time

For making a comparison in computational times, each method was applied to the pulse mentioned before and computed at ten different end times; namely, $t_{end} \in \{6, 12, 18, 24, 30, 36, 42, 48, 54, 60\}$ minutes. For every time t_{end} each method was applied a hundred times for which the computational time was measured. Then, the average was calculated from all the hundred computational times. These averages are plotted in the figures below. Figure 7.1 shows the computational times for the Upwind method and Figure 7.2 shows the computational times for the Lax-Wendroff method. The average ratios of the computational times of the Dynamic wave model versus the Diffusion wave and the Kinematic wave model are given in Table 7.1.

For both the Upwind method and the Lax-Wendroff method, the computational times of the kinematic and the diffusion wave are comparable. The computational times of the dynamic wave, however, are significantly larger. Note that the computational times of the Upwind method and the Lax-Wendroff method are very similar.

Method \\ Ratio	Dynamic : Kinematic	Dynamic : Diffusion
Upwind	16	15
Lax-Wendroff	16	15

Table 7.1: The average ratios between the computational times of the Dynamic wave versus the Diffusion wave and the Kinematic wave. The Kinematic wave is 16 times faster than the Dynamic wave and the Diffusion wave is 15 times faster than the Dynamic wave.

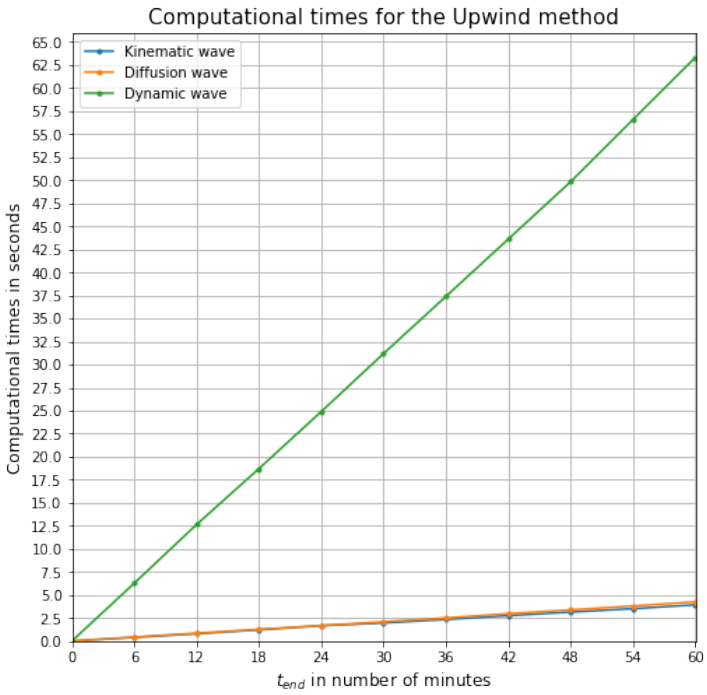

Figure 7.1: The computational times in seconds of the Upwind method applied to the kinematic wave, the diffusion wave and the dynamic wave.

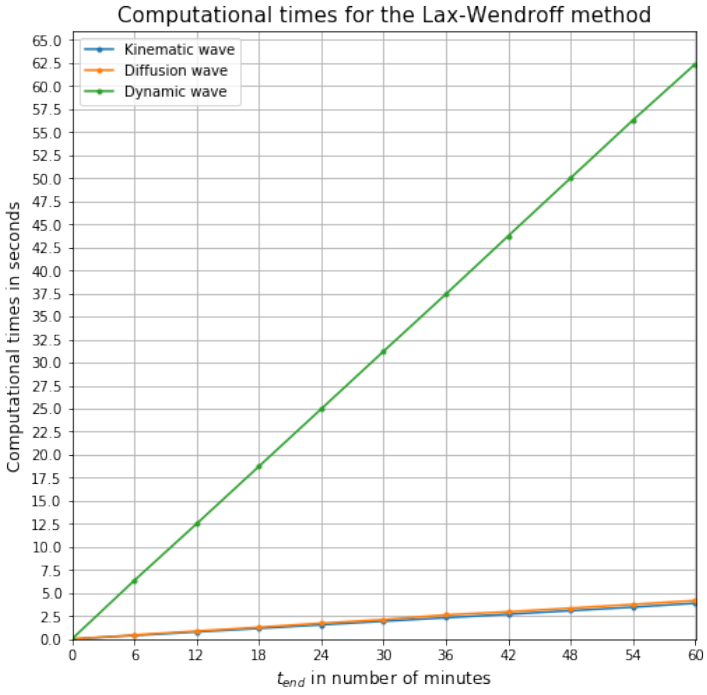

Figure 7.2: The computational times in seconds of the Lax-Wendroff method applied to the kinematic wave, the diffusion wave and the dynamic wave.

7.3. Representation of reality

Kinematic wave The kinematic wave model assumes long and flat waves. The model produces waves flowing downstream only in which the flow is steady and uniform within each differential length. As a result, each wave travels downstream with a constant speed and does not attenuate as it flows.

The kinematic wave needs a channel bed slope to model water movement. The water flow velocity is therefore dependent on the slope steepness. To imitate the water flow in Dutch polders using the kinematic wave, an artificial channel bed slope is to be implemented. A channel bed slope of 1 meter per kilometer is applied which seems to give reasonable water flow velocities. It is a point for further research to examine further whether this choice of slope is a feasible decision.

Diffusion wave The diffusion wave is very similar to the kinematic wave. It assumes long and flat waves which also flow downstream only. The diffusion wave also needs a channel bed slope to model wave movement. The diffusion wave attenuates as it moves downstream. Accordingly, it can model backwater effects. Therefore it resembles water movement in a Dutch ditches network more closely than the kinematic wave model. In this thesis, the diffusion wave was not applied successfully to all cases yet. This is also a point for further research.

Dynamic wave Naturally, the dynamic wave models water flow as close to reality as possible since it uses the full shallow water equations. Waves move in both directions and attenuate as they move. The equations model water flow in a very detailed manner, with turbulent flows as well. It models the water flow more precisely than may be necessary for this purpose.

7.4. Modeling difficulty

Fool-proof modeling Successful implementation of the full shallow water equations is a fool-proof type of modeling water flow because of its realistic representation. It does not take many interpretation steps. The kinematic and the diffusion waves, however, are easier to implement but require the modeler to take more care with interpretation.

Difficulty of the numerical methods The kinematic and the diffusion wave equations are conservation laws to which a one dimensional nonlinear numerical solution method is applied. The nonlinearity in the solution method is expressed in different wave speeds for every grid cell.

The diffusion wave is trickier to model than the kinematic wave. The numerical methods are the same, however, the flux function is different. The flux function in the diffusion wave equation involves a square root. The value inside the square root can easily take negative values which results in non-real solutions and breaking numerical method. For implementing the diffusion wave, linearization of the square root could be considered to prevent these negative values in the square root.

The full shallow water equations are modeled with a method for nonlinear systems of equations. Naturally, this complicates the numerical methods because the operations now have to be done on a system of two equations. In addition, two boundary conditions need to be specified; one on either side. Stability issues appear easily when these boundary conditions are not implemented correctly.

7.5. Accuracy

The accuracy of the numerical solutions depends on the type of numerical method that is used. Here, the Upwind method and the Lax-Wendroff were implemented. The Upwind method has an accuracy of the order Δt. It smooths the solution visibly. The Lax-Wendroff method has a higher accuracy of the order $\mathcal{O}(\Delta t)^2$ but produces oscillation in the results. Here, implementation of both methods turn out to have similar accuracies overall. This is likely because the Upwind method smooths the data and the Lax-Wendroff method produces oscillatory behavior which makes them comparable overall. Also, rounding errors may have come into play.

One could think of applying high resolution methods to achieve more accurate results without the oscillations. A high resolution method uses a second order accurate method for the smooth parts of the data and it uses a first order accurate method for the non smooths parts of the data. Accordingly, a high-resolution limiter defines when to use which linear method depending on the smoothness of the data [12]. Various high-resolution limiters could be explored, such as the minmod or the van Leer limiter. This was beyond the scope of this research for which the focus was more on exploring the different wave modeling approaches available.

8

Modeling kinematic wave networks

8.1. General

The next step toward a water flow model for a ditches network is to create a simple network and test the developed numerical methods. In order to do so, confluence conditions need to be determined for junctions of waterways. These conditions are simple for the kinematic wave equation, however, they become more complex for the full shallow water equations. Here, the focus will be on a simple kinematic wave network. The comparison will be made with SOBEK, which is a program that implements the full shallow water equations for water networks.

8.2. Implementation of a kinematic wave network

A simple waterway network is considered consisting of six ditches and two junctions, as illustrated in Figure 8.1.

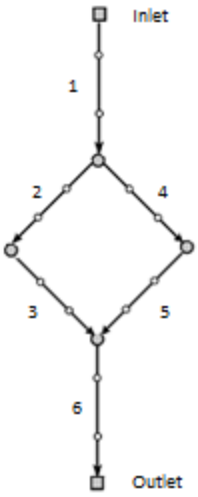

Figure 8.1: The test network which is the network under consideration for this chapter.

8.2.1. Initial conditions and boundary conditions

As was discussed in the earlier chapters, an initial solution needs to be defined at all grid cells in order to apply any numerical approximation method. Therefore, all points in the network in Figure 8.1 are assigned the downstream depth at the network's outlet.

The boundary conditions are defined similarly to what was discussed for the kinematic wave in a straight ditch in Chapter 4. The values of the network's inlet and outlet are the boundary conditions. The inlet boundary condition is assigned a value for the discharge, which can be calculated into a water depth value which is needed for the approximation method. The outlet boundary condition is assigned a fixed depth value.

8.2.2. Confluence conditions

Two confluence conditions are implemented. First of all, the water depths should be equal in the waterway junctions. For example, the downstream water depth of ditch 1 equals the upstream water depths of ditch 2 and ditch 4 in Figure 8.1. This is implemented by taking the downstream boundary values of ditch 1 and using them as the upstream boundary values for ditch 2 and ditch 4. A similar method is applied to all the other connections in the network.

Additionally, the sum of the discharge values in junctions should be constant in order to satisfy the continuity principle. The discharge flowing into the junction should equal the discharge flowing out of the junction. This means for the example above that $Q_{1,\text{out}} = Q_{2,\text{in}} + Q_{4,\text{in}}$.

8.2.3. Results

The kinematic wave model is tested on the ditches network shown in Figure 8.1 with equal widths of the ditches; namely, a width of 1 meter. The surface water gradient in a polder ditches network from the inlet to the outlet is generally 1 cm per 1 kilometer. Therefore, in the kinematic wave network model, a channel bed slope of 1 centimeter per kilometer is assumed to begin with.

Equal cross sections The kinematic wave is governed by gravity, hence the water flow is fully dependent on the channel bed slopes. Therefore, an average slope of $S_0 = \frac{0.01\,\text{m}}{1000\,\text{m}}$ is implemented to imitate the water flow in the zero sloped ditches in a Dutch polder network. This means that the difference in water bed height between the water inlet point and the water outlet point is $\frac{0.01\,\text{m}}{1000\,\text{m}}$ times the total length that the water travels. The lengths of the ditches are displayed in Table 8.1.

Ditch number	Length (m)
1	1000
2	1414
3	1414
4	1414
5	1414
6	1000

Table 8.1: The lengths of the ditches in the network shown in Figure 8.1

Therefore, the water travels a total length of 4828 meters from the inlet to the outlet. Thus the channel bed height differs in 4.828 cm between the inlet and the outlet. Now, given that the total channel bed slope is 4.828 cm over the total 4828 meters, the channel bed slopes for each ditch are engineered such that discharges in the junctions satisfy the confluence conditions. Because of the waterway separation from ditch 1 to ditch 2 and 3, the discharges in ditch 2 and 3 are different from the discharge in ditch 1. Hence, the channel bed

slopes are also different. The following paragraphs discuss how these channel bed slopes are engineered. Table 8.2 show these resulting slopes for this network.

The discharge is defined and calculated by

$$q = \frac{1}{n_m} S_0^{1/2} \frac{(A)^{5/3}}{(R)^{2/3}} \tag{8.1}$$

$$= \frac{1}{n_m} S_0^{1/2} \frac{(Bh)^{5/3}}{(2h+B)^{2/3}} \tag{8.2}$$

For waterway junctions, the cross sections A, the hydraulic radii R and the Gauckler-Manning coefficient n_m of the three connected ditches are equal. The channel bed slope S_0 is the only non-fixed variable. In the waterway separation in the network, the discharges in ditch 2 and 4 equal half the discharge in ditch 1 because of the specified confluence conditions. Hence, resulting in a slope in ditch 2 and 3 of one fourth of the slope in ditch 1 as is illustrated in the calculation below

$$\frac{1}{2} \times q = \frac{1}{2} \times \text{constant} \times S_0^{1/2} \tag{8.3}$$

$$= \text{constant} \times (\frac{1}{4} S_0)^{1/2} \tag{8.4}$$

Applying the kinematic wave to the network requires to set the artificial channel bed slopes according to the expected discharge values in the ditches using the confluence conditions. Using the ditches lengths given in Table 8.1 and the assumption that the total slope over the total length is 4.828 cm, one attains to the following channel bed slope values

Ditch number	Slope
1,6	$\frac{1.784 \text{ cm}}{1000 \text{ m}}$
2,3,4,5	$\frac{0.446 \text{ cm}}{1000 \text{ m}}$

Table 8.2: The artificial slopes for the ditches given in 8.1.

Figures 8.2, 8.3 and 8.4 show the results for the water levels and the discharges computed for a total time of 2,5 days so 60 hours. Here, the inflow discharge at the inlet is set to $Q_{1,\text{in}} = 0.05376 \text{ m}^3/\text{s}$ which equals a water depth of 1.04828 meters. The initial water levels above a given horizontal datum are set to 1 meter everywhere, meaning that the water depths are determined by subtraction of the channel bed slope from these water levels. The spatial calculation points are placed at every 100 meters. The time step was set to 12 minutes. This time step was manually optimized such that the CFL number has a value of 0.4467 in ditch 1 and ditch 6 which have the highest slopes and reach the CFL limit faster. 0.4467 is close to the CFL number's limiting value for stability; namely, the CFL number should be smaller than $\frac{1}{2}$ as was discussed in Section 4.3.4. Note that it is important to satisfy the CFL limit for every value along the entire computations. Hence, the Python scripts check this CFL limit for every computation and break when the CFL limit is exceeded.

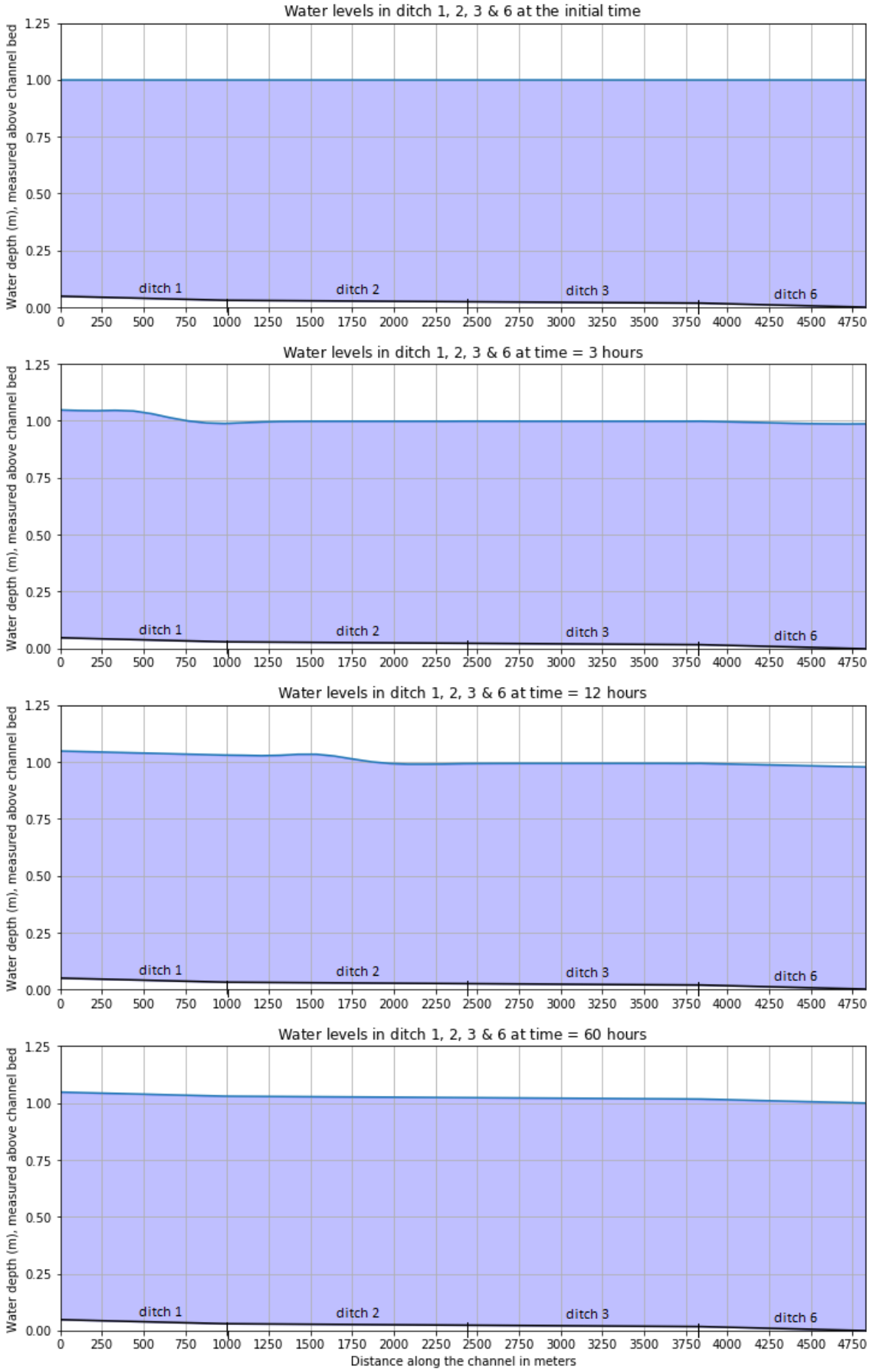

Figure 8.2: The results for water levels of the left branch of the network including ditches 1, 2, 3 and 6.

To zoom into the water behavior and its depths, Figure 8.3 shows the same as in the previous figure but now zoomed in and at slightly different times. This simplifies the comparison with SOBEK later on in this section.

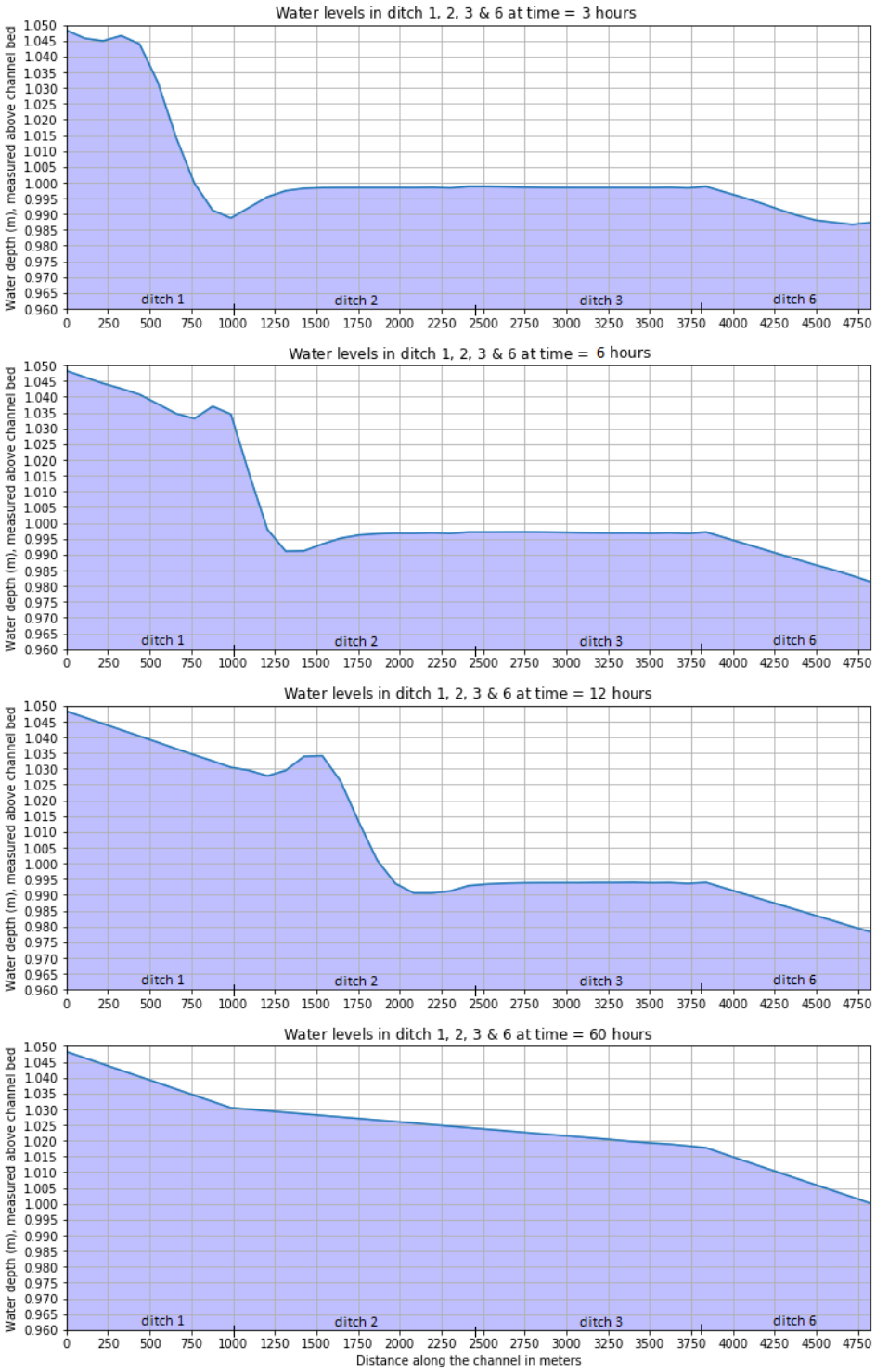

Figure 8.3: The results for water levels of the left branch of the network including ditches 1, 2, 3 and 6.

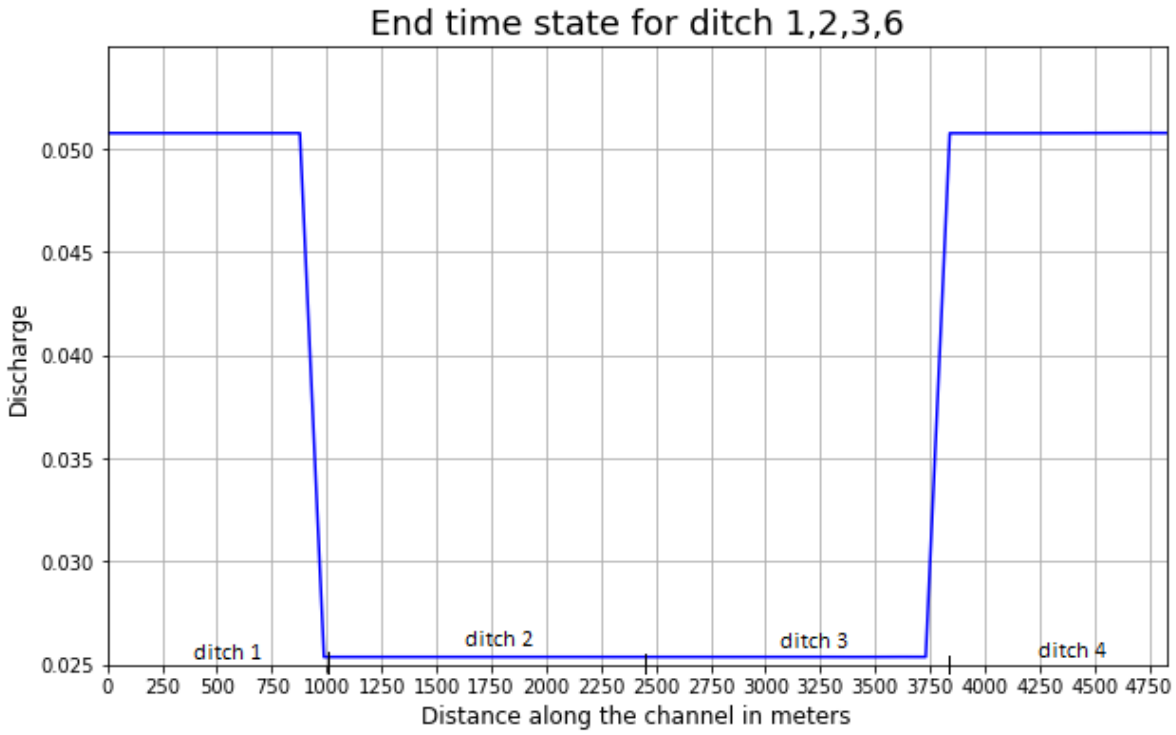

Figure 8.4: The results for the discharges of the left branch of the network including ditches 1, 2, 3 and 6.

Clearly, the water flow is very slow for a channel bed slope of 1 centimeter per kilometer. It takes 60 hours for the wave to travel through the entire ditches network. Let us compare with the results when doing the same simulation in SOBEK.

Non-equal cross sections When the widths of the ditches vary, (8.3) does not simply hold. Depending on the widths, new discharge-slope relations need to be found for the separating ditches. This is a point for further research.

8.3. Implementation with SOBEK

SOBEK is a water modeling tool used for many applications such as flood forecasting, salt intrusion and surface water quality. It has a wide variety of features which makes it possible to model a water system's behavior in a very detailed manner [15]. These detailed features add complexity and computational time. Naturally, it is possible to implement simple systems such as the case discussed above as well. This application is made in this section to compare the performance of the kinematic wave network with SOBEK's full shallow water equations network.

8.3.1. Confluence conditions

The confluence conditions for the full shallow water equations are more complex than those for the kinematic wave equation. A confluence condition should be implemented for both equations; a continuity of flow condition and a conservation of momentum condition. The latter brings the difficulties, since momentum cannot be simply added up since the momentum direction needs to be taken into account. The SOBEK suite technical reference manual explains how this is done [15].

8.3.2. Results

Similar to the kinematic wave network case above, the spatial calculation points are placed at every 100 meters and the time step is set to 1 minute. The channel bed slope $S_0 = 0$ is implemented. After 12 hours a stable and fixed water depth and discharge situation is obtained. To enable comparison with the kinematic wave network, the time of 60 hours is considered. The values are shown in Figure 8.5, Figure 8.6 and Figure 8.7.

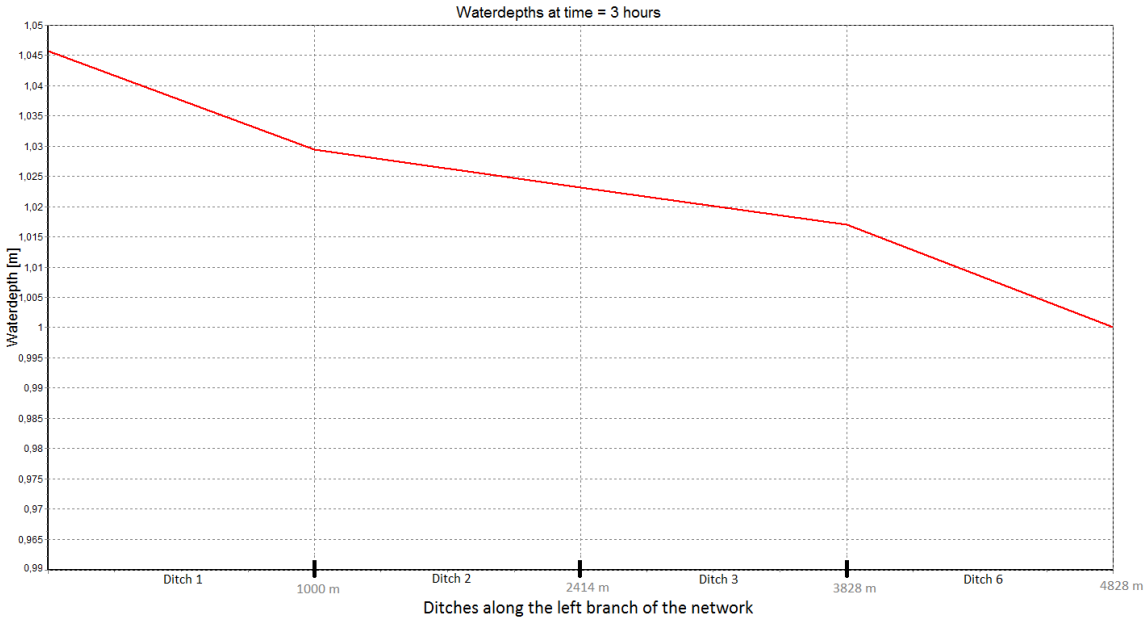

Figure 8.5: The water depths computed by SOBEK for the left branch of the network, showing values for the ditches 1,2,3 and 6 after 3 hours time.

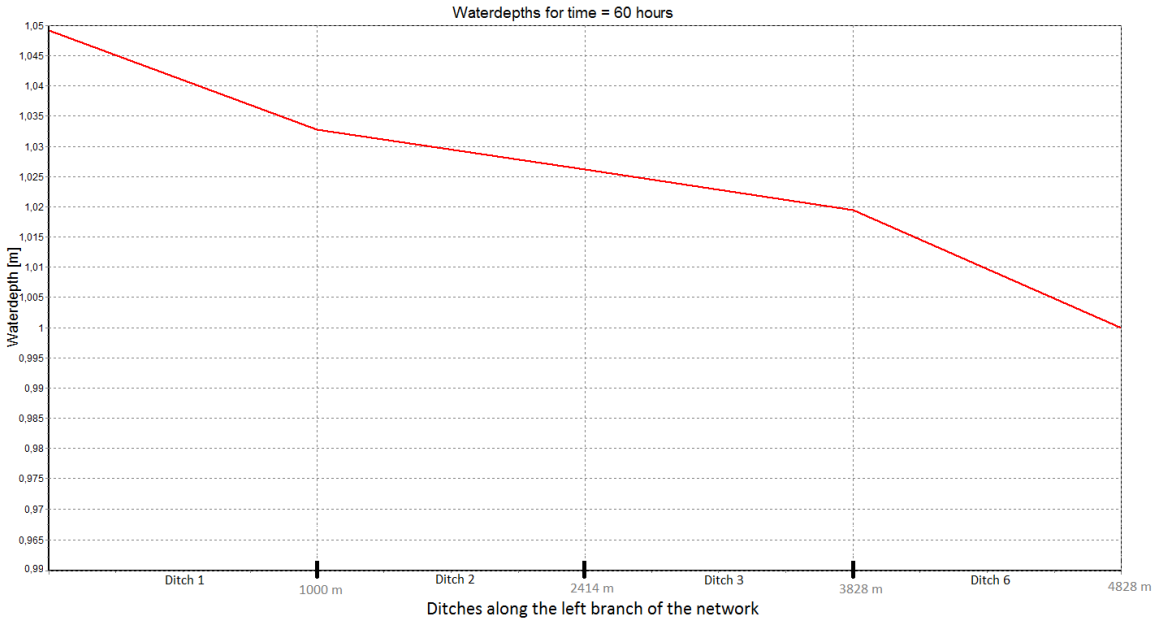

Figure 8.6: The water depths computed by SOBEK for the left branch of the network, showing values for the ditches 1,2,3 and 6 after 60 hours time.

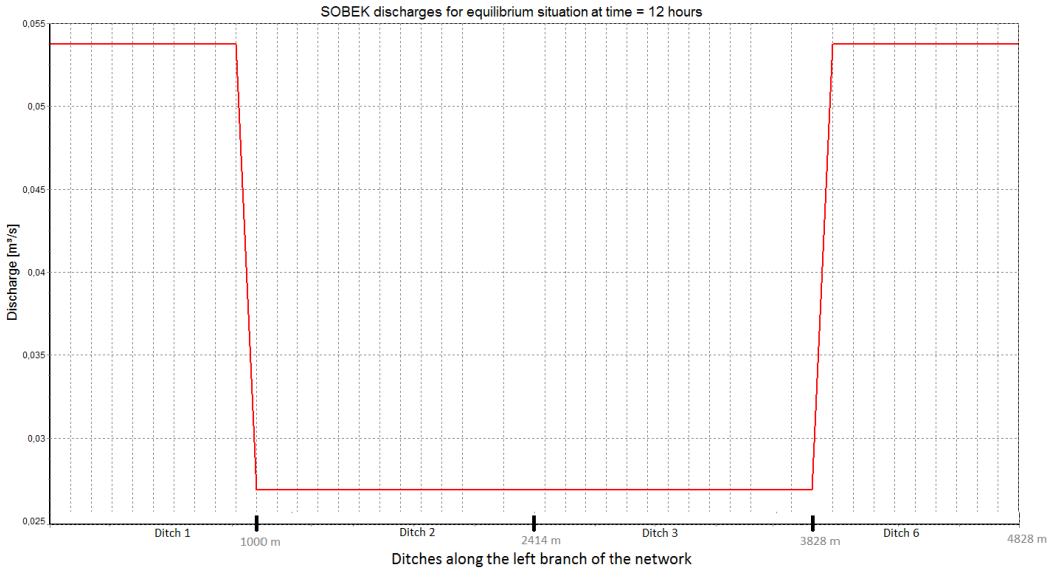

Figure 8.7: The discharges computed by SOBEK for the left branch of the network, showing values for the ditches 1,2,3 and 6 at the equilibrium state after 12 hours.

8.4. A comparison

The water flow in the network was computed by the kinematic wave and SOBEK's full shallow water equations. A simple comparison between the results will be made in the following paragraphs. For both methods, a total tieme of 60 hours was computed in the previous sections. First of all, the end values for the water depths and discharges are compared. See Tables 8.3 and 8.4 for the values of the water depths above datum and the discharges at the time 60 hours.

	Inlet	Inflow point ditch 2	Inflow point ditch 3	Inflow point ditch 6	Outlet
Kinematic	1.048	1.030	1.024	1.018	1.000
SOBEK	1.049	1.033	1.026	1.020	1.000

Table 8.3: Comparison between the water depths (in meters) above datum between the kinematic wave network and SOBEK's full shallow water equations at time = 60 hours.

	Inlet	Inflow point ditch 2	Inflow point ditch 3	Inflow point ditch 6	Outlet
Kinematic	0.0508	0.0254	0.0254	0.0508	0.0508
SOBEK	0.0538	0.0269	0.0269	0.0538	0.0538

Table 8.4: Comparison between the discharge values (in cubed meters per second) above datum between the kinematic wave network and SOBEK's full shallow water equations at time = 60 hours.

The end water depths are comparable. Assuming that SOBEK is very accurate, the kinematic wave values are off by a maximum of 3 millimeters. The discharges are slightly different. This is due to the artificial channel bed slopes which decrease the kinematic wave water depths above the channel bed in comparison with SOBEK. When the water depths are smaller, the discharges are also smaller.

Computational time For the kinematic wave, the Lax-Wendroff numerical finite volume method was applied. Table 8.5 shows the computational times for the kinematic wave network and SOBEK's full shallow

water equations network.

The kinematic wave computational times increase with computing longer periods of times. SOBEK takes a constant time to compute the results. This is because it runs many additional processes around the actual wave computations. These additional processes require a constant amount of time. The wave computations increase in computational speed, however this is not significant yet for computing these periods of time. SOBEK's computational times will likely increase for more than 5 days. Unsurprisingly, SOBEK is fast when computing a simple network. It is a program which has been under development and computational speed optimization for many years.

	12 hrs	24 hrs	1.5 day	2 day	2.5 days	3 days	3.5 days	4 days	4.5 days	5 days
Kinematic	0.75 s	1.50 s	2.25 s	3.00 s	3.78 s	4.49 s	5.25 s	5.99 s	6.74 s	7.48 s
SOBEK	5 s	5 s	5 s	5 s	5 s	5 s	5 s	5 s	5 s	5 s

Table 8.5: The computational times for the two network programs applied to the simple waterway network with various times t_{end}. Both methods were implemented using time steps of 1 minute. Note that SOBEK only gives the computational time in seconds accuracy.

Accuracy SOBEK is known for its highly accurate results due to its implementation of the full shallow water equations and optimization of the numerical methods. How does the kinematic wave compare to this? First of all, the kinematic wave results in a less realistic representation of water flow than the full shallow water equations. The kinematic wave is governed by the channel bed slope and only flows in one direction. The full shallow water equations also model water flow with zero slopes and produce waves in both directions, which is a more realistic representation of the water flow situation in a ditches network. However, the kinematic wave can still be useful when implemented with care. The kinematic wave yields a simple and suitable algorithm, if the necessary parameters are chosen with care.

As was seen in the computed networks, the water flows significantly slower in the kinematic wave network compared to SOBEK's network. This is due to the very small values for the channel bed slopes which are set to an average of 1 cm per kilometer giving a value of $S_0 = \frac{0.01}{1000}$. Now, when searching for a similar water velocity to the velocities in SOBEK's network, one can experimentally set the average channel bed slope to 1 meter per kilometer and arrive at similar results. However, adjusting the channel bed slopes in this way should be tested or theorized properly before it can be implemented appropriately.

The Upwind and the Lax-Wendroff methods are also limited in their accuracy. The numerical methods used for approximating the kinematic wave equation could be improved upon yielding more computational speed and higher accuracies. As was mentioned in Section 7.4, high resolution methods could be implemented to develop a numerical solution method which combines first-order and second-order methods to optimize accuracies.

9

Conclusion

9.1. Conclusion

The aim of this thesis was to develop a simple and fast model for surface water flow in a ditches network of a Dutch polder. The model would preferably be fast enough to eventually run on a mobile phone. The available modeling programs for this purpose generally model water flow using the detailed shallow water equations which quickly lead to high computational times. Instead of the full shallow water equations, the simpler kinematic wave equation was chosen as the main focus of this research. Would the kinematic wave still give a general idea of the water flow in a ditches network while reducing computational times drastically?

In order to find out, two finite volume numerical solutions methods were developed to solve the hyperbolic kinematic wave equation on a straight ditch. The Upwind method is the simplest method with a theoretical accuracy of the order $\mathcal{O}(\Delta t)$. It gives smooth and smeared results. The Lax-Wendroff method is more accurate with a theoretical accuracy of the order $\mathcal{O}(\Delta t^2)$. It gives accurate results but also causes oscillatory behavior in the solutions. Both methods were implemented with first order accuracies because the Upwind method smooths solutions and the Lax-Wendroff method causes oscillatory behavior. Both methods worked successfully for the kinematic wave equation resulting in comparable computational times.

Additionally, finite volume numerical methods were developed to solve the diffusion wave equation and the full shallow water equations, also known as the dynamic wave model. Hence, a comparison was made between the kinematic wave and the two other modeling approaches. The kinematic wave flow is generated by the channel bed slope and its waves move downstream only. Since the channel bed slopes are generally zero in a ditches network in a Dutch polder, artificial channel bed slope were used. The kinematic wave yields similar computational times and modeling results as the diffusion wave equation. The only difference is that the diffusion wave could include backwater effects. Unfortunately, the numerical methods for the diffusion wave were not successfully implemented for all possible cases. On the other hand, the dynamic wave was implemented successfully with zero channel bed slopes. It yields significantly higher computational times compared to the kinematic and the diffusion wave; namely, the dynamic waves requires 15 to 16 times longer computational times in comparison with the diffusion wave and the kinematic wave respectively. Thus, the dynamic wave is the most realistic representation of surface water flow while requiring higher computational times. Therefore, implementing the developed methods for the dynamic wave may not be feasible for the fast water flow model on a mobile phone.

A further step was made by computing the kinematic wave in a simple hypothetical ditches network with equal cross sections. The artificial channel bed slope of 1 centimeter per kilometer was chosen to imitate the stream gradient in a ditches network in a Dutch polder. The water moves very slowly with this slope. Therefore, a higher artificial channel bed slope is needed for a more accurate representation of the water flow. A comparison with SOBEK was made which shows that SOBEK is very fast and compares well to the computational times of the implementation of the kinematic wave. This is unsurprisingly so since SOBEK has been under development and numerical speed optimization for many years.

In summary, the kinematic wave and the diffusion wave require much smaller computational times when comparing the developed numerical methods for a straight ditch. In comparison to the dynamic wave, the kinematic wave and the diffusion wave take care in choosing an appropriate channel bed slope and with interpreting the results. When comparing the developed kinematic wave network with SOBEK, the kinematic wave is not necessarily faster than SOBEK which implements the dynamic wave model.

9.2. Recommendations for future research

In order to successfully apply the kinematic wave to ditches networks in Dutch polders, more testing needs to be done to find an appropriate channel bed slope. Additionally, how to connect ditches with different cross sections is a point for further research in the networks.

The kinematic wave network may be extended to a diffusion wave network which incorporates backwater effects. This may be desirable once structures, such as dams, will be included in the water flow model. More research needs to be done to applying the diffusion wave without breaking of the solutions. Some literature is available on how to model diffusion wave networks which can be explored further, see [16–19].

With regard to computational speeds and accuracies, only two simple and straightforward numerical methods were implemented. Higher accuracies and lower computational times may be achieved by implementing high-resolution numerical methods.

Finally, SOBEK seems to model very accurate water flow behavior with low computational times for the simple network under consideration. It may be worth exploring the applicability of SOBEK for modeling the water flow, and even water quality parameters for saline water, for the desired web and phone application.

Bibliography

[1] L. Tolk and J. Velstra, "Spaarwater, pilots rendabel en duurzaam agrarisch watergebruik in een verziltende omgeving van de waddenregio," Acacia Institute, Tech. Rep., 2016. [Online]. Available: http://www.spaarwater.com/content/27227/download/clnt/67009_Spaarwater_hoofdrapport_2016.pdf

[2] A. M. van Dam, O. A. Clevering, W. Voogt, T. G. L. Aendekerk, and M. P. van der Maas, "Leven met Zout Water," Praktijkonderzoek Plant \& Omgeving B.V., Tech. Rep., 2007. [Online]. Available: http://www.stowa.nl/Upload/nieuws/LevenmetZoutWater_DeelrapportZouttolerantieLandbouwgewassen.pdf

[3] E. van Essen, B. Snellen, J. Kroes, and L. Stuyt, "Sociaal-economisch spoor verzilting Noord-Nederland," Acacia Institute, Tech. Rep., 2011. [Online]. Available: http://www.acaciadata.com/doc/Eindrapport-278-Sociaal-EconomischspoorverziltingNoord-Nederland.pdf

[4] G. Van Staveren and J. Velstra, "Verzilting van landbouwgronden in Noord-Nederland in het perspectief van de effecten van klimaatsverandering," Acacia Institute, Tech. Rep., 2012. [Online]. Available: http://www.acaciadata.com/doc/Syntheserapport-278-VerziltingvanlandbouwgrondeninNoordNederland.pdf

[5] T. W. Sturm, *Open channel hydraulics*. Boston: McGraw-Hill, 2010.

[6] M. H. Chaudhry, *Open-Channel Flow*. Boston, MA: Springer US, 2008. [Online]. Available: http://link.springer.com/10.1007/978-0-387-68648-6

[7] P. J. J. F. Torfs, *Open channel flow [Course notes]*. Wageningen (the Netherlands): Hydrology and Quantitive Water Management Group, 2013.

[8] V. T. Chow, D. R. Maidment, and L. W. Mays, *Applied Hydrology*, mcgraw-hil ed. New York: McGraw-Hill, 1988.

[9] J. E. Miller, "Basic Concepts of Kinematic-Wave Models," *U.S. Geological Survey Professional Paper 1302*, 1983. [Online]. Available: https://pubs.usgs.gov/pp/1302/report.pdf

[10] J. F. Cruise, M. M. M. M. Sherif, and V. P. V. P. Singh, *Elementary hydraulics*. Toronto: Thomson/Nelson, 2007.

[11] E. P. Querner, "Aquatic weed control within an integrated water management framework," DLO Winand Staring Centre, Wageningen (the Netherlands), Tech. Rep., 1993. [Online]. Available: http://www.querner.eu/site/Ned-onderzoek/Report-67-PhD-Querner-juni1993.pdf

[12] R. LeVeque, *Finite Volume Methods for Hyperbolic Problems*. Cambridge: Cambridge University Press, 2002.

[13] P. Eagleson, *Dynamic hydrology*. New York: McGraw-Hill, 1970.

[14] C. Vuik, F. Vermolen, M. v. Gijzen, and M. Vuik, *Numerical methods for ordinary differential equations*. DAP, Delft Academic Press, 2015.

[15] Deltares, "D-Flow 1D (SOBEK 3); technical reference manual," Delft, 2017. [Online]. Available: http://content.oss.deltares.nl/delft3d/manuals/D-Flow1D_Technical_Reference_Manual.pdf

[16] V. M. Ponce, "Generalized diffusion wave equation with inertial effects," *Water Resources Research*, vol. 26, no. 5, pp. 1099–1101, 5 1990. [Online]. Available: http://doi.wiley.com/10.1029/WR026i005p01099

[17] M. A. Sabur and P. M. Steffler, "A conservative diffusion wave flood routing scheme for channel networks," vol. 23, pp. 566–570, 1996.

[18] V. P. Singh, "Accuracy of kinematic wave and diffusion wave approximations for space independent flows," *Hydrological Processes*, vol. 8, no. 1, pp. 45–62, 1994.

[19] G. E. Blandford and L. E. Ormsbee, "A diffusion wave finite element model for channel networks," *Journal of Hydrology*, vol. 142, no. 1-4, pp. 99–120, 1993.

[20] L. Rossman and W. C. Huber, "Storm Water Management Model Reference Manual Volume II – Hydraulics," Tech. Rep. January, 2016.

Appendices

A

Results of the method of manufactured solutions

A.1. MMS for the advection equation

As was previously discussed in Section 4.4.2, consider the advection equation assuming the wave speed $\bar{u} = 1$

$$w_t + w_x = 0 \tag{A.1}$$

and assuming the solution $w(x,t) = -\sin(t-x)$. Comparing the solution $w(x,t) = -\sin(t-x)$ with the numerical results when the upwind scheme and the Lax-Wendroff results in small differences between the real solution and the numerically computed solution as is shown in Table A.1 and Table A.2. Thus, the developed Upwind and Lax-Wendroff numerical methods are verified.

Table A.1: Error between manufactured analytical solution and the upwind numerical solution for the advection equation, measured by the distance function $d(x, y) = |y - x|$ where y is the assumed solution and x the numerical solution. The number of intervals was set to $nx = 24$, with the interval distance $\Delta x = \frac{2\pi}{24} \approx 0.26$ and the time step $\Delta t = \Delta x \approx 0.26$.

Interval \\ Time	Time = 10 s	Time = 60 s	Time = 10 mins	Time = 60 mins
$\mathcal{C}_1$	0.00000000e+00	0.00000000e+00	0.00000000e+00	0.00000000e+00
$\mathcal{C}_2$	0.00000000e+00	4.63943333e-18	1.09801057e-13	3.93796107e-13
$\mathcal{C}_3$	0.00000000e+00	0.00000000e+00	0.00000000e+00	0.00000000e+00
$\mathcal{C}_4$	1.72084569e-15	6.21724894e-15	8.03801470e-14	0.00000000e+00
$\mathcal{C}_5$	1.75517282e-15	0.00000000e+00	0.00000000e+00	0.00000000e+00
$\mathcal{C}_6$	0.00000000e+00	0.00000000e+00	2.94209102e-14	0.00000000e+00
$\mathcal{C}_7$	0.00000000e+00	0.00000000e+00	0.00000000e+00	1.17683641e-13
$\mathcal{C}_8$	0.00000000e+00	0.00000000e+00	0.00000000e+00	0.00000000e+00
$\mathcal{C}_9$	0.00000000e+00	1.77635684e-15	5.68434189e-14	0.00000000e+00
$\mathcal{C}_{10}$	0.00000000e+00	0.00000000e+00	0.00000000e+00	0.00000000e+00
$\mathcal{C}_{11}$	0.00000000e+00	0.00000000e+00	9.84212711e-14	0.00000000e+00
$\mathcal{C}_{12}$	2.22044605e-16	0.00000000e+00	0.00000000e+00	4.54748241e-13
$\mathcal{C}_{13}$	4.44089210e-16	6.88338275e-15	1.13677721e-13	0.00000000e+00
$\mathcal{C}_{14}$	0.00000000e+00	7.12150917e-15	0.00000000e+00	0.00000000e+00
$\mathcal{C}_{15}$	0.00000000e+00	0.00000000e+00	0.00000000e+00	0.00000000e+00
$\mathcal{C}_{16}$	0.00000000e+00	0.00000000e+00	8.03801470e-14	0.00000000e+00
$\mathcal{C}_{17}$	9.11063175e-16	0.00000000e+00	0.00000000e+00	0.00000000e+00
$\mathcal{C}_{18}$	0.00000000e+00	3.55271368e-15	2.94209102e-14	0.00000000e+00
$\mathcal{C}_{19}$	0.00000000e+00	1.88737914e-15	0.00000000e+00	0.00000000e+00
$\mathcal{C}_{20}$	0.00000000e+00	0.00000000e+00	2.94209102e-14	2.27373675e-13
$\mathcal{C}_{21}$	0.00000000e+00	0.00000000e+00	0.00000000e+00	0.00000000e+00
$\mathcal{C}_{22}$	2.22044605e-16	0.00000000e+00	5.68434189e-14	0.00000000e+00
$\mathcal{C}_{23}$	0.00000000e+00	5.10702591e-15	0.00000000e+00	0.00000000e+00
$\mathcal{C}_{24}$	0.00000000e+00	0.00000000e+00	9.84767823e-14	1.05518852e-17

Table A.2: Error between manufactured analytical solution and the Lax-Wendroff numerical solution for the advection equation, measured by the distance function $d(x, y) = |y - x|$ where y is the assumed solution and x the numerical solution. The number of intervals was set to $nx = 24$, with the interval distance $\Delta x = \frac{2\pi}{24} \approx 0.26$ and the time step $\Delta t = \Delta x \approx 0.26$.

Interval \\ Time	Time = 10 s	Time = 60 s	Time = 10 mins	Time = 60 mins
$\mathcal{C}_1$	0.00000000e+00	0.00000000e+00	0.00000000e+00	0.00000000e+00
$\mathcal{C}_2$	1.11022302e-16	5.55111512e-17	1.09801057e-13	3.93685085e-13
$\mathcal{C}_3$	5.55111512e-17	3.43271324e-17	1.11022302e-16	1.11022302e-16
$\mathcal{C}_4$	5.55111512e-17	0.00000000e+00	8.03801470e-14	-1.11022302e-16
$\mathcal{C}_5$	0.00000000e+00	0.00000000e+00	0.00000000e+00	1.11022302e-16
$\mathcal{C}_6$	5.55111512e-17	0.00000000e+00	2.95319325e-14	0.00000000e+00
$\mathcal{C}_7$	0.00000000e+00	1.11022302e-16	0.00000000e+00	1.17683641e-13
$\mathcal{C}_8$	1.11022302e-16	2.22044605e-16	0.00000000e+00	0.00000000e+00
$\mathcal{C}_9$	0.00000000e+00	0.00000000e+00	5.68434189e-14	0.00000000e+00
$\mathcal{C}_{10}$	1.11022302e-16	1.11022302e-16	0.00000000e+00	5.55111512e-17
$\mathcal{C}_{11}$	0.00000000e+00	0.00000000e+00	9.85878046e-14	0.00000000e+00
$\mathcal{C}_{12}$	0.00000000e+00	1.11022302e-16	5.55111512e-17	4.54748241e-13
$\mathcal{C}_{13}$	0.00000000e+00	1.11022302e-16	1.13733232e-13	5.55111512e-17
$\mathcal{C}_{14}$	1.11022302e-16	5.55111512e-17	5.55111512e-17	1.11022302e-16
$\mathcal{C}_{15}$	1.11022302e-16	2.28847549e-17	1.11022302e-16	1.11022302e-16
$\mathcal{C}_{16}$	4.99600361e-16	9.43689571e-16	8.04911693e-14	0.00000000e+00
$\mathcal{C}_{17}$	1.14423775e-17	0.00000000e+00	0.00000000e+00	2.22044605e-16
$\mathcal{C}_{18}$	5.55111512e-17	0.00000000e+00	2.91988655e-14	2.22044605e-16
$\mathcal{C}_{19}$	3.33066907e-16	0.00000000e+00	0.00000000e+00	0.00000000e+00
$\mathcal{C}_{20}$	4.44089210e-16	0.00000000e+00	2.94209102e-14	2.27373675e-13
$\mathcal{C}_{21}$	0.00000000e+00	0.00000000e+00	5.69544412e-14	0.00000000e+00
$\mathcal{C}_{22}$	2.22044605e-16	1.11022302e-16	0.00000000e+00	0.00000000e+00
$\mathcal{C}_{23}$	0.00000000e+00	0.00000000e+00	9.84767823e-14	0.00000000e+00
$\mathcal{C}_{24}$	0.00000000e+00	2.22044605e-16	0.00000000e+00	1.05518852e-17

A.2. MMS and Richardson extrapolation for the kinematic wave equation

For the numerical solutions methods of the kinematic wave equation, the solution $h(x,t) = \frac{3}{2} - \sin(t-x)$ was assumed and tested using the method of manufactured solutions. The number of intervals was set to $nx = 24$, with the interval distance $\Delta x = \frac{2\pi}{24} \approx 0.26$ and the time step $\Delta t = \frac{1}{2}\Delta x \approx 0.19$ which gives that $dt \approx 0.8dx$ so that the CFL number is approximately 0.467 which is close to the CFL number limit of $\frac{1}{2}$. Finding the accuracy of the kinematic wave equation was done by applying the Richardson extrapolation method mentioned on page 34 in [14]. Thus, $\Delta x/2$ and $\Delta x/4$ were used for calculating the error decreasing when the time and spatial discretization steps are halved. The end time was set to $t_{end} = 60$ minutes. For a first order method, the error is halved when the discretization steps are halved. Both the Upwind and the Lax-Wendroff error results show the trend of halving errors. Therefore, they both seem to be first order accurate with the implementation in discussed in this report.

Table A.3: The errors between the assumed solution and the Upwind computed solution for various sizes of discretization steps.

Interval \\ Discretization step	4*dx, 4*dt	2*dx, 2*dt	dx, dt
$\mathcal{C}_1$	0.	0.	0.
$\mathcal{C}_2$	0.17369475	0.08499694	0.04199028
$\mathcal{C}_3$	0.13892861	0.06646339	0.03245277
$\mathcal{C}_4$	0.09372526	0.04266917	0.02026978
$\mathcal{C}_5$	0.0425915	0.01598825	0.00665761
$\mathcal{C}_6$	-0.0096362	-0.0110356	-0.00707655
$\mathcal{C}_7$	-0.05820829	-0.03590286	-0.01967886
$\mathcal{C}_8$	-0.09884965	-0.05621173	-0.02997175
$\mathcal{C}_9$	-0.12824089	-0.06974228	-0.03667034
$\mathcal{C}_{10}$	-0.14461412	-0.07507699	-0.03850854
$\mathcal{C}_{11}$	-0.1482038	-0.07270915	-0.03563874
$\mathcal{C}_{12}$	-0.14112019	-0.06527868	-0.03053773
$\mathcal{C}_{13}$	-0.12646008	-0.05593389	-0.02564782
$\mathcal{C}_{14}$	-0.10704485	-0.04631733	-0.02126209
$\mathcal{C}_{15}$	-0.08456088	-0.03632977	-0.01666567
$\mathcal{C}_{16}$	-0.05963832	-0.02536961	-0.01147911
$\mathcal{C}_{17}$	-0.03264976	-0.01330161	-0.00574815
$\mathcal{C}_{18}$	-0.00434449	-0.00050588	0.00029176
$\mathcal{C}_{19}$	0.02430966	0.01249486	0.0063663
$\mathcal{C}_{20}$	0.05244841	0.02521862	0.01220361
$\mathcal{C}_{21}$	0.07899467	0.03715073	0.01754476
$\mathcal{C}_{22}$	0.10235509	0.04775322	0.02223065
$\mathcal{C}_{23}$	0.12071304	0.05655167	0.02627789
$\mathcal{C}_{24}$	0.13243535	0.0630699	0.02977102

Table A.4: The errors between the assumed solution and the Lax-Wendroff computed solution for various sizes of discretization steps.

Interval \\ Discretization step	4*dx, 4*dt	2*dx, 2*dt	dx, dt
$\mathcal{C}_1$	0.	0.	0.
$\mathcal{C}_2$	0.16339566	0.08000215	0.0394534
$\mathcal{C}_3$	0.10824812	0.05176241	0.02512597
$\mathcal{C}_4$	0.03906401	0.01623646	0.00720653
$\mathcal{C}_5$	-0.03446838	-0.02108135	-0.01147674
$\mathcal{C}_6$	-0.10362214	-0.05386576	-0.02798459
$\mathcal{C}_7$	-0.15511937	-0.07702111	-0.03973067
$\mathcal{C}_8$	-0.17106449	-0.08955727	-0.04474303
$\mathcal{C}_9$	-0.14093435	-0.08352196	-0.04217669
$\mathcal{C}_{10}$	-0.07393109	-0.05060554	-0.02818864
$\mathcal{C}_{11}$	0.003544	-0.00403032	-0.00334939
$\mathcal{C}_{12}$	0.06414476	0.03355772	0.01700393
$\mathcal{C}_{13}$	0.09433795	0.05231431	0.02674497
$\mathcal{C}_{14}$	0.09629468	0.05449647	0.02827321
$\mathcal{C}_{15}$	0.07969156	0.04611005	0.02439817
$\mathcal{C}_{16}$	0.05328202	0.03246175	0.01761174
$\mathcal{C}_{17}$	0.02142281	0.01687424	0.00996235
$\mathcal{C}_{18}$	-0.01494438	0.00133963	0.00229545
$\mathcal{C}_{19}$	-0.05674435	-0.01371411	-0.00573005
$\mathcal{C}_{20}$	-0.09628702	-0.02981864	-0.01441895
$\mathcal{C}_{21}$	-0.1238853	-0.04807316	-0.02276719
$\mathcal{C}_{22}$	-0.1227471	-0.06326988	-0.02810947
$\mathcal{C}_{23}$	-0.07377536	-0.06241208	-0.03002378
$\mathcal{C}_{24}$	-0.06927864	-0.03045867	-0.02338367